HHS Public Access

Author manuscript

Mol Microbiol. Author manuscript; available in PMC 2018 September 01.

Published in final edited form as:

Mol Microbiol. 2017 September ; 105(5): 755–776. doi:10.1111/mmi.13733.

Bactericidal peptidoglycan recognition protein induces oxidative stress in *Escherichia coli* through a block in respiratory chain and increase in central carbon catabolism

Des R. Kashyap, **Marcin Kuzma**, **Dominik A. Kowalczyk**, **Dipika Gupta**, and **Roman Dziarski***

Indiana University School of Medicine–Northwest, Gary, IN 46408, USA

Summary

Mammalian Peptidoglycan Recognition Proteins (PGRPs) kill both Gram-positive and Gram-negative bacteria through simultaneous induction of oxidative, thiol, and metal stress responses in bacteria. However, metabolic pathways through which PGRPs induce these bactericidal stress responses are unknown. We screened Keio collection of *Escherichia coli* deletion mutants and revealed that deleting genes for respiratory chain flavoproteins or for tricarboxylic acid (TCA) cycle resulted in increased resistance of *E. coli* to PGRP killing. PGRP-induced killing depended on the production of hydrogen peroxide, which required increased supply of NADH for respiratory chain oxidoreductases from central carbon catabolism (glycolysis and TCA cycle), and was controlled by cAMP-Crp. Bactericidal PGRP induced a rapid decrease in respiration, which suggested that the main source of increased production of hydrogen peroxide was a block in respiratory chain and diversion of electrons from NADH oxidoreductases to oxygen. CpxRA two-component system was a negative regulator of PGRP-induced oxidative stress. By contrast, PGRP-induced thiol stress (depletion of thiols) and metal stress (increase in intracellular free Zn^{2+} through influx of extracellular Zn^{2+}) were mostly independent of oxidative stress. Thus, manipulating pathways that induce oxidative, thiol, and metal stress in bacteria could be a useful strategy to design new approaches to antibacterial therapy.

Abbreviated Summary

*correspondence: rdziar@iun.edu, phone: 219-980-6535, fax: 219-980-6566.

Supporting information

Additional Supporting Information may be found in the online version of this article at the publisher's web-site.

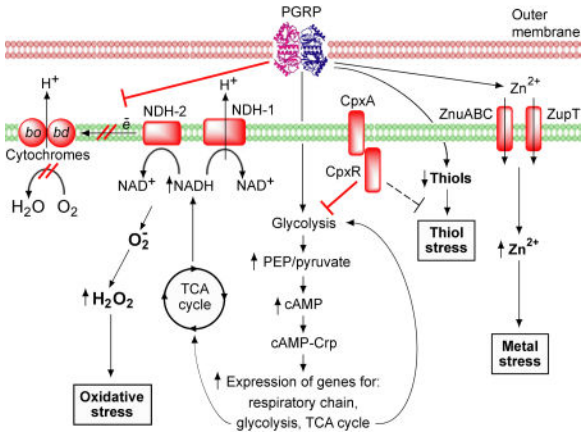

Bactericidal PGRP induces oxidative stress through a block in respiratory chain, which diverts electrons from NADH oxidoreductases to O_2, generates H_2O_2, and results in decreased respiration. Production of H_2O_2 depends on increased supply of NADH from cAMP-Crp-controlled glycolysis and TCA cycle. CpxRA is a negative regulator of PGRP-induced oxidative stress. PGRP-induced thiol stress (depletion of thiols) and metal stress (increase in intracellular free Zn^{2+} through influx of extracellular Zn^{2+}) are mostly independent of oxidative stress.

Keywords

peptidoglycan recognition protein; oxidative stress; thiol stress; metal stress; respiration; cAMP-Crp; CpxRA

Introduction

Peptidoglycan Recognition Proteins (PGRPs or PGLYRPs) are evolutionarily conserved innate immunity molecules homologous to bacteriophage type 2 amidases, present in animals and humans (Royet and Dziarski, 2007; Dziarski *et al.*, 2016). Mammals have four PGRP genes, *PGLYRP1, PGLYRP2, PGLYRP3*, and *PGLYRP4*, which code for soluble secreted proteins. PGLYRP1, PGLYRP3, and PGLYRP4 are directly bactericidal for both Gram-positive and Gram-negative bacteria (Tydell *et al.*, 2002, 2006; Lu *et al.*, 2006; Wang *et al.*, 2007), whereas PGLYRP2 is an enzyme, peptidoglycan amidohydrolase (Gelius *et al.*, 2003; Wang *et al.*, 2003). All PGRPs have one or two PGRP domains with a binding site specific for muramyl-penta-, tetra-, or tri-peptide fragment of bacterial peptidoglycan (Royet and Dziarski, 2007; Dziarski *et al.*, 2016). In addition, mammalian PGRPs have another binding site specific for bacterial lipopolysaccharide (LPS) located outside the peptidoglycan-binding groove (Tydell *et al.*, 2006; Sharma *et al.*, 2011).

Bacterial killing is initiated by binding of PGRP to bacteria. In Gram-positive bacteria, PGRPs preferentially bind to muramyl peptides exposed by peptidoglycan-lytic endopeptidases at the separation sites of the newly formed daughter cells (Kashyap *et al.*, 2011). In Gram-negative bacteria, PGRPs bind uniformly to the entire outer membrane (Kashyap *et al.*, 2011), because of the ability of PGRPs to bind LPS (Tydell *et al.*, 2006; Sharma *et al.*, 2011).

PGRPs do not enter the cytoplasm, but rather exert their bactericidal effect through induction of exaggerated stress responses in bacteria (Kashyap *et al.*, 2011). Efficient PGRP killing of both Gram-positive and Gram-negative bacteria requires simultaneous induction by PGRPs of oxidative, thiol, and metal stress responses in bacteria (Kashyap *et al.*, 2014).

PGRP-induced oxidative stress is manifested by increased production of hydrogen peroxide (H_2O_2) and hydroxyl radicals ($HO^{\bullet}$) and high induction of oxidative stress response genes, including OxyR and SoxR regulons in *Escherichia coli* and PerR regulon in *Bacillus subtilis* (Kashyap *et al.*, 2011; 2014). Production of H_2O_2 and $HO^{\bullet}$ is required for PGRP-induced killing, because under anaerobic conditions, when H_2O_2 and $HO^{\bullet}$ are not produced, PGRPs are not bactericidal, but only bacteriostatic (Kashyap *et al.*, 2014). The requirement for H_2O_2 and $HO^{\bullet}$ in PGRP-induced killing is further supported by inhibition of PGRP-induced killing by dipyridyl, which inhibits $HO^{\bullet}$ production (Kashyap *et al.*, 2011), and by a greater sensitivity to PGRP killing of Δ*recA E. coli* mutants (deficient in DNA repair) and Hpx^{-} *E. coli* and *B. subtilis* mutants (deficient in catalases and hydroxyperoxidases) (Kashyap *et al.*, 2014).

PGRP-induced thiol (disulfide) stress in both *E. coli* and *B. subtilis* is manifested by depletion of over 90% of intracellular thiols and by a great increase in the expression of thiol stress response genes, including many genes for chaperones and protein quality control (Kashyap *et al.*, 2014). Depletion of thiols is required for PGRP-induced killing, because thiourea (which protects from thiol depletion) diminishes PGRP-induced bacterial killing (Kashyap *et al.*, 2011; 2014).

PGRP-induced metal stress is manifested by increases in intracellular free (labile) Zn^{2+} in *E. coli* and both Zn^{2+} and Cu^{+} in *B. subtilis*, and also by a great increase in the expression of metal efflux and metal detoxification genes (Kashyap *et al.*, 2014). PGRP-induced metal stress is required for PGRP killing of bacteria, because selective chelation of Zn^{2+} or Cu^{+} completely abolishes PGRP killing in both *E. coli* and *B. subtilis* (Wang *et al.*, 2007; Kashyap *et al.*, 2014).

Although induction of each of these stress responses is required for PGRP-induced killing, each stress response individually is not sufficient for bacterial killing and has only bacteriostatic effect. Efficient killing requires simultaneous induction of all threes stress responses, i.e., oxidative, thiol, and metal stress (Kashyap *et al.*, 2014). Similar killing can be recapitulated by the simultaneous treatment of bacteria with agents that induce H_2O_2 production, depletion of thiols, and elevation of intracellular metal concentrations. PGRP-induced stress responses lead to cessation of all biosynthetic reactions in bacteria, including protein, RNA, DNA, and intracellular peptidoglycan synthesis, membrane depolarization, and bacterial death (Kashyap *et al.*, 2011).

The mechanism of induction of oxidative, thiol, and metal stress by PGRPs in bacteria, the sequence of their induction, and their relation to each other, are unknown. This knowledge is important not only for greater understanding how these innate immunity proteins kill bacteria, but also for future applications to rationally design more efficient antibacterial agents, and for resolving some of the recent controversies regarding the role of oxidative

stress in bacterial killing (Kohanski *et al.*, 2007, 2008; Brynildsen *et al.*, 2013; Ezraty *et al.*, 2013; Liu and Imlay, 2013; Keren *et al.*, 2013; Mahoney and Silhavy, 2013; Dwyer *et al.*, 2014, 2015; Lobritz *et al.*, 2015; Imlay, 2015).

We performed this study to identify metabolic pathways through which PGRP induces oxidative, thiol, and metal stress responses in bacteria and to determine whether these stress responses are induced through the same single pathway or different independent pathways. We show that in *E. coli* PGRP induced oxidative stress through a block in respiratory chain and likely premature diversion of electrons to O_2, resulting in increased H_2O_2 production and decreased respiration. Production of H_2O_2 depended on increased supply of NADH from cAMP-Crp-controlled central carbon catabolism. CpxRA two-component system was a negative regulator of PGRP-induced oxidative stress. By contrast, PGRP-induced thiol stress (depletion of thiols) and metal stress (increase in intracellular free Zn^{2+}) were both mostly independent of oxidative stress and CpxRA.

Results

Deletion of genes for respiratory chain flavoproteins, TCA cycle, Crp, or cAMP increases resistance to PGRP killing

We screened the entire *E. coli* Keio library of 3884 single gene deletion mutants to find mutants with increased resistance to PGRP killing (Fig. S1A). We did not find any mutants completely resistant to PGRP, if resistance is defined as growth in the presence of PGRP concentrations that are bactericidal for parental bacteria. However, we identified 14 partially resistant mutants with statistically significant higher survival than the parental strain and the ratio of survival of PGRP-treated Δ mutant *versus* parental strain of 10 to 100 (Fig. 1A and Table S1). 13 of these mutants were in genes coding for proteins involved in flavin-catalyzed redox reactions, including 5 mutants in genes coding for proteins that participate in oxidation of NADH in the respiratory chain (*nuoE, nuoG, nuoJ, nuoK*, and *ndh*), 5 for enzymes from the TCA cycle (*sucD, sucB, lpdA, icd*, and *sdhD*), and 3 for other oxidoreductases (*frdC, betA*, and *ybdK*) (Fig. 1A, Table S1).

To verify these results, we generated mutants in several key genes (*nuoEF, ndh, sucB*, and *sucD*) in another *E. coli* strain, MG1655, and we tested their sensitivity to PGRP killing. All four mutants constructed by us were significantly more resistant to PGRP killing compared with the parental MG1655 strain (Fig. 1B), which verifies the findings with Keio mutants. These results suggested that the reactions performed by the products of these genes are critical steps in PGRP killing.

Eleven genes out of the top 14 genes, whose deletion increased resistance to PGRP killing, are under the positive control of the cAMP receptor protein (Crp), eight directly and three indirectly: two through catabolite repressor activator (Cra), which is a positive regulator of Crp, and one through Fis, which is regulated by Crp (Table S1). cAMP-Crp complex is a transcriptional dual regulator of central carbon catabolism and energy production that senses insufficient generation of energy sources in the cells and up-regulates expression of genes for energy production (Supplementary text). Therefore, we next tested whether Crp and cAMP are required for PGRP-induced killing. Indeed, deletion of *crp* or *cyaA* completely

abolished bactericidal effect of PGRP for *E. coli* (Fig. 1B). *cyaA* codes for adenylate cyclase, an enzyme that generates cAMP, and cAMP complexes with Crp to form the active transcription factor. Because *crp* or *cyaA* deletion mutants grew very slowly, it could be argued that their slow growth was the reason for their increased resistance to PGRP killing. However, in our screening there were also some other mutants that grew equally slowly but were efficiently killed by PGRP, which suggests that the resistance effect of *crp* or *cyaA* deletion was selective for these mutations, and not solely caused by the slow growth. Thus, these results indicate that both Crp and cAMP are required for bactericidal effect of PGRP.

PGRP-induced generation of H_2O_2 requires respiratory chain, TCA cycle, Crp, and cAMP

We next tested the role of the above-identified genes and the reactions carried out by their products in the PGRP-induced generation of H_2O_2, which we have previously shown to be required for PGRP killing of bacteria (Kashyap *et al.*, 2014). PGRP treatment of aerobically growing *E. coli* induced high level of H_2O_2 production that peaked at 15 min and declined by 30 min (Fig. 2A). Treatment with paraquat as a positive control (which generates O_2^- and H_2O_2 directly after being reduced to radical cations by complex I) (Cochemé and Murphy, 2008; Imlay, 2013) induced a similar increase in H_2O_2 production that also peaked at 15 min, but did not decline at 30 min. *E. coli* similarly treated with BSA as a negative control had low levels of H_2O_2 throughout the incubation period, as expected.

PGRP-induced increase in H_2O_2 was mostly abolished in all Keio mutants with deletions of genes for either respiratory chain (*nuo* and *ndh*) or TCA cycle (*sucB, sucD, lpdA*, and *icd*), and was decreased by about half in two other redox flavoprotein mutants, fumarate reductase (*frdC*) and choline dehydrogenase (*betA*) (Fig. 2B). Similarly, PGRP-induced H_2O_2 production was abolished in *nuoEF, ndh, sucB*, and *sucD* deletion mutants that we constructed in *E. coli* MG1655 (Fig. 2C), which verifies the results obtained with the Keio mutants. These results are consistent with the higher resistance of these mutants to PGRP killing, and with greater resistance of a double *nuoA ndh* deletion mutant to PGRP killing (Fig. 1A, Table S1).

We next tested the role of Crp and cAMP in PGRP-induced generation of H_2O_2. Treatment of *crp* or *cyaA* deletion mutants with PGRP did not result in an increase in H_2O_2 production (Fig. 2C). These results show that Crp and *cyaA* (cAMP) are required for PGRP-induced generation of H_2O_2.

E. coli mutants with deletions of genes for the respiratory chain (*nuo* and *ndh*), the TCA cycle (*sucB, sucD, icd*, and *lpdA*), *crp* and *cyaA*, or two other redox proteins (*frdC* and *betA*), when grown with BSA (as a control), had similar or somewhat higher levels of H_2O_2 compared with the parental BW25113 and MG1655 strains (Fig. 2B,C), consistent with previous reports for *nuo, ndh*, and *frd* mutants (Seaver and Imlay, 2004; Korshunov and Imlay, 2010). Because these mutants treated with PGRP had drastically lower levels of H_2O_2 than the parental strains, these results indicate that the main sources of PGRP-induced H_2O_2 are different from the sources of the low-level H_2O_2 produced in control cells growing without PGRP.

PGRP induces increased expression of Crp-controlled genes for central carbon catabolism and respiratory oxidoreductases

The requirement for Crp, cAMP, and cAMP-Crp-controlled genes in PGRP-induced killing suggested that treatment of *E. coli* with PGRP may increase the expression of Crp-controlled genes, including the genes for utilization of glycerol, glycolysis, TCA cycle, and respiratory chain oxidoreductases. We tested this prediction by comparing expression of these genes using whole genome expression arrays in BSA- (control) and PGRP-treated *E. coli* under the conditions of severe PGRP-induced oxidative, thiol, and metal stress (Kashyap *et al.*, 2014). Analysis of these arrays (NCBI GEO accession number GSE44211) revealed significant increases in expression of five genes that participate in glycerol utilization in lower glycolysis (*glpK, glpD, gapA, gpmM*, and *eno*, as glycerol was the energy source in our medium) and 17 TCA cycle genes (*aceE, lpdA, gltA, acnA, acnB, icd, sucA, sucB, sucC, sucD, sdhA, sdhB, fumA, fumB, fumC, mdh*, and *mqo*) in PGRP-treated compared with BSA-treated *E. coli* (Fig. 3 and Table S2). The reactions catalyzed by the products of these genes are shown in Fig. S2. All of these TCA cycle genes and several glycerol utilization genes are positively controlled by cAMP-Crp (Fig. 3 and Table S2) (Karp *et al.*, 2017; Shimada *et al.*, 2011). These results suggest greater utilization of glycerol and increased glycolysis and TCA cycle in PGRP-treated cells.

We also determined whether PGRP-treated *E. coli* also had increased expression of genes for respiratory oxidoreductases, which were required for full sensitivity to PGRP-killing (Fig. 1 and Table S1) and for PGRP-induced increase in H_2O_2 (Fig. 2B,C). PGRP treatment significantly increased expression of *ndh* and 8 out of 13 *nuo* genes after 30 min (Fig. 3 and Table S2) or 15 min (Fig. S3). The *nuo* operon is positively regulated by cAMP-Crp, and both *nuo* operon and *ndh* are positively regulated by Fis, which is controlled by Crp (Karp *et al.*, 2017; Shimada *et al.*, 2011). A high (17-fold) increase in *ndh* expression in PGRP-treated bacteria indicates a higher demand for NDH-2 than NDH-1 to oxidize the excess of NADH generated in glycolysis and TCA cycle. PGRP treatment also significantly increased expression of genes for two other oxidoreductases, fumarate reductase (*frdC*) and choline dehydrogenase (*betA*) (Fig. 3 and Table S2), consistent with higher resistance of *frdC* and *betA* deletion mutants to PGRP killing (Fig. 1A and Table S1) and with significantly diminished PGRP-induced H_2O_2 production in these mutants (Fig. 2B).

PGRP induces an increase in NADH, phosphoenolpyruvate, and cAMP

To identify the sources and the pathways that result in PGRP-induced generation of H_2O_2, and also in thiol and metal stress, we next performed epistatic and biochemical analysis of the role of central carbon catabolism in PGRP-induced stress responses.

We first tested whether treatment with PGRP changes the concentrations of NADH and NAD^+ in *E. coli*, because several mutants with increased resistance to PGRP killing involved genes whose products participate in generation of NADH in the TCA cycle or oxidation of NADH in the respiratory chain (Fig. 1, Table S1), and because NADH could be the source of reducing power for generation of H_2O_2. Under aerobic conditions bacteria produce NADH in energy-generating reactions (such as glycolysis and TCA cycle, Fig. S2) and then oxidize

it to NAD^+ in the respiratory chain using NADH:ubiquinone oxidoreductases I and II (NDH-1 coded in *E. coli* by *nuoA-N*, and NDH-2 coded by *ndh*).

Treatment of *E. coli* with PGRP induced rapid increase in NADH level and NADH/NAD^+ ratio, which peaked in 15 min and were not observed in control BSA-treated cells, yielding significantly higher NADH levels and NADH/NAD^+ ratio in PGRP-treated than in control cells at 5, 15, and 30 min (Fig. 4A). The level of NAD^+ did not change in both PGRP- and BSA-treated bacteria throughout the 60 min incubation period. This PGRP-induced increase in NADH levels and NADH/NAD^+ ratio correlated with and preceded the PGRP-induced increase in H_2O_2 (Fig. 2A). Thus, oxidation of NADH to NAD^+ by the respiratory chain could be the source of reducing power for PGRP-induced generation of H_2O_2.

The two main sources of NADH in *E. coli* grown in our experiments aerobically with glycerol as the energy source are components of central carbon catabolism, lower glycolysis and TCA cycle (Fig. S2 and Supplemental text). Thus, we then tested whether PGRP induces an increase in central carbon catabolism, by measuring phosphoenolpyruvate (PEP) and PEP/pyruvate ratio. PGRP treatment of *E. coli* resulted in a rapid and significant increase in PEP concentration and PEP/pyruvate ratio with a peak at 5 min (Fig. 4B), which indicates increased glycolysis.

We then tested production of cAMP, because cAMP is required for the activity of Crp (Supplemental text). PGRP treatment of *E. coli* resulted in a significant increase in intracellular cAMP, which peaked in 5 min (Fig. 4C), which indicates the predicted activation of adenylate cyclase. Thus, the peaks of PGRP-induced increases in the PEP/pyruvate ratio and in cAMP (5 min) preceded and thus were up-stream from the PGRP-induced increases in NADH and H_2O_2, which peaked at 15 min (Figs. 2A and 4A).

PGRP-induced changes in NADH/NAD^+ and PEP/pyruvate ratios in PGRP-resistant mutants

We next tested the role of NADH-oxidizing respiratory chain enzymes (NDH-1 and NDH-2), TCA cycle enzymes, and their regulators (cAMP and Crp) in PGRP-induced increased production of NADH, PEP, and cAMP by epistatic analysis using deletion mutants that were more resistant to PGRP killing.

The NADH/NAD^+ ratios were significantly decreased in PGRP-treated *sucB* and *sucD* deletion mutants (both Keio and ours) and also in our *crp* and *cyaA* mutants, compared with the NADH/NAD^+ ratios in PGRP-treated parental strains (Fig. 5A). These results are consistent with the predicted accumulation of NAD^+ and the decreased capacity of these mutants to reduce it to NADH (Fig. S2). Lower NADH/NAD^+ ratios in these mutants are also consistent with decreased PGRP-induced production of H_2O_2 in these mutants due to lower availability of NADH for the respiratory chain. Both *ndh* mutants had increased NADH/NAD^+ ratios in PGRP-treated cells compared with parental strains (Fig. 5A), which reflects significantly decreased ability of *ndh* mutants to oxidize NADH to NAD^+. These results suggest that NDH-2 is the main NADH-oxidizing enzyme in PGRP-treated cells, consistent with a high PGRP-induced increase in *ndh* expression (17-fold, Fig. 3). By contrast, the NADH/NAD^+ ratios were significantly decreased in PGRP-treated *nuoE, nuoG*,

and *nuoEF* deletion mutants compared with PGRP-treated parental strains (Fig. 5A), suggesting no significant role of NDH-1 in NADH oxidation in PGRP-treated cells and possibly diminished ability of *nuo* mutants to generate NADH. Thus, diminished H_2O_2 production and killing in PGRP-treated *nuo* mutants could be due to decreased NADH/NAD^+ ratio, similar to the TCA cycle mutants. Changes in the NADH/NAD^+ ratios correlated better with the PGRP resistant phenotype of the mutants than the absolute levels of NADH, which was especially evident in *crp* and *cyaA* mutants (Fig. 5A), because of increased baseline levels of NADH.

PGRP did not induce an increase in PEP and PEP/pyruvate ratios in *nuoE, nuoEF, nuoG, ndh, sucB*, and *sucD* deletion mutants (both Keio and ours), whereas in *crp* and *cyaA* mutants there was a decrease in PEP and PEP/pyruvate ratios, in contrast to significant increases in both PEP and PEP/pyruvate ratios in PGRP-treated parental strains (Fig. 5B). These results indicate lower metabolic activity and inability to increase glycolysis following PGRP treatment in all these mutants, consistent with their increased resistance to PGRP killing and decreased PGRP-induced H_2O_2 production (Figs. 1 and 2).

We also tested PGRP-induced induction of cAMP production in PGRP-resistant mutants, because cAMP is required for activation of Crp, which would show whether the defect in these mutants is up-stream or down-stream from Crp. PGRP treatment of *nuoE, nuoEF, nuoG, ndh, sucB*, and *sucD* mutants (both Keio and ours), as well as their parental strains, induced similar increases in cAMP, whereas, as expected, *cyaA* mutant (deficient in adenylate kinase) had very low level of cAMP (Fig. 5C). The *crp* deletion mutant also had very low level of cAMP, which is unexpected, because Crp is a negative regulator of *cyaA*. These results confirm that control of cAMP production is up-stream from the reactions catalyzed by *nuo, ndh*, and *suc* gene products, consistent with the findings that in *E. coli* growing on glycerol (which is the energy source in our medium) activation of adenylate cyclase is controlled by glycerol-3-phosphate (Eppler *et al.*, 2002).

PGRP induces a block in respiratory chain

Based on the requirement for the TCA cycle and respiratory NADH oxidoreductases for PGRP-induced generation of H_2O_2, we considered two hypotheses that could explain how H_2O_2 is generated in PGRP-treated *E. coli*. The first hypothesis postulated that H_2O_2 is produced as a by-product of increased rate of respiration and increased flux of electrons through the respiratory chain to the cytochromes, due to increased supply of NADH and increased oxidation of NADH by the respiratory chain NADH oxidoreductases. This hypothesis predicted that PGRP should induce an increase in O_2 consumption, because a large amount of O_2 would have to be reduced to H_2O to generate an accompanying large increase in H_2O_2 as a by-product of incomplete O_2 reduction (which is an infrequent event).

The second hypothesis postulated that H_2O_2 is produced by diversion of electrons from NADH oxidoreductases directly to O_2 due to a block of electron transfer from NADH oxidoreductases to the cytochromes. This hypothesis predicted that PGRP would cause a decrease in O_2 consumption, because a block in electron transfer to the cytochromes would result in a decrease in cytochrome-catalyzed reduction of O_2 to H_2O.

Thus, we next tested these hypotheses by measuring in real time PGRP-induced changes in O_2 consumption rate with the Seahorse XFp analyzer, which uses label-free solid-state sensor cartridges in a microplate format (Lobritz *et al.*, 2015; Saini *et al.*, 2016). Treatment of *E. coli* with PGRP induced rapid decrease in O_2 consumption rate, which was already significantly lower at 5 min and continued to decrease to near base-line level for 30 min (Fig. 6A). By contrast, BSA-treated control cells maintained stable O_2 consumption rate throughout the entire 60-min incubation period (Fig. 6A). These results support our second hypothesis and indicate that PGRP causes a block in the respiratory chain, likely leading to electron backup on NADH oxidoreductases.

Simultaneously with O_2 consumption rate, we also measured in real time the extracellular acidification rate (ECAR, using Seahorse XFp analyzer), which reflects total H^+ production from carbon catabolism. BSA-treated control cells steadily increased the ECAR throughout the entire 60-min incubation period, which reflected healthy cell growth. By contrast, in PGRP-treated cells, ECAR increased only during the first 5 min of incubation, indicating initial acceleration of metabolism, and then declined and remained low during the remaining incubation (Fig. 6B). Plotting O_2 consumption rate *versus* ECAR illustrates the total cell energy phenotype and shows high-energy state (respiration and metabolism) for the control cells incubated with BSA, and low-energy phenotype for the PGRP-treated cells (Fig. 6C), consistent with eventual energy depletion and impending death.

PGRP-induced depletion of thiols is mostly independent of respiratory chain, TCA cycle, and generation of H_2O_2

PGRP also induces severe depletion of intracellular thiols in bacteria (referred to as thiol stress), and this thiol depletion is required for efficient bacterial killing by PGRP (Kashyap *et al.*, 2014). However, the mechanism of PGRP-induced depletion of thiols is unknown. Because PGRP does not enter the cytoplasm (Kashyap *et al.*, 2011) and also because PGRP by itself is not a thiol-oxidizing electrophile, the simplest hypothesis to explain PGRP-induced thiol depletion would be through induction of intracellular reactive oxygen species (ROS), as thiol stress is often considered a consequence and a component of oxidative stress (Leichert *et al.*, 2003; Müller *et al.*, 2013). Here we tested this hypothesis for PGRP-induced depletion of thiols, by using deletion mutants for respiratory chain, TCA cycle, their regulators, and other flavoproteins that had severely diminished PGRP-induced H_2O_2 production (Fig. 2B,C).

PGRP treatment of parental strains resulted in 91–93% depletion of thiols. Similar treatment of mutants deficient in respiratory chain genes (*nuo* and *ndh*), or in TCA cycle genes (*sucB, sucD, icd*, and *lpdA*), or in genes for other redox flavoproteins (*frdC* and *betA*), on average resulted in 85 ± 2% depletion of intracellular thiols, which was still significant and only 10% less efficient than in parental strains (Fig. 7). Therefore, 90% of overall thiol depletion was still present in mutants for respiratory chain (*nuo* and *ndh*), TCA cycle (*sucB, sucD, icd*, and *lpdA*), and other redox flavoproteins (*frdC* and *betA*) genes, and thus was mostly independent of these genes. Therefore, this thiol depletion was also mostly independent of PGRP-induced H_2O_2 production, which was abolished or severely diminished in these mutants.

In mutants for the regulators of central carbon metabolism (*crp* and *cyaA*), PGRP induced 62% to 54% depletion of thiols, which was still significant, but shows that about 30–40% of PGRP-induced thiol depletion is dependent on cAMP-Crp (Fig. 7).

PGRP-induced increase in intracellular Zn^{2+} is independent of respiratory chain, TCA cycle, and generation of H_2O_2

In addition to strong oxidative and thiol stress, PGRP also induces metal stress, manifested in *E. coli* by an increase in intracellular free Zn^{2+} and strong up-regulation of metal efflux and detoxification mechanisms (Kashyap *et al.*, 2014). To investigate the role of oxidative stress and respiratory chain, TCA cycle, and other redox flavoproteins in PGRP-induced increase in intracellular free Zn^{2+}, we tested induction of intracellular free Zn^{2+} by PGRP in several mutants with deleted genes required for PGRP-induced oxidative stress.

PGRP treatment in mutants deficient in respiratory chain genes (*nuo* and *ndh*), in TCA cycle genes (*sucB, sucD, icd*, and *lpdA*), in regulators of central carbon metabolism (*crp* and *cyaA*), or in genes for other redox flavoproteins (*frdC* and *betA*) resulted in similar increases in intracellular free Zn^{2+} as in parental bacteria (Fig. 8A). These results show that PGRP-induced increase in intracellular free Zn^{2+} is independent of the respiratory chain, TCA cycle, cAMP-Crp, and two redox flavoproteins (*frdC* and *betA*), and also independent of PGRP-induced production of H_2O_2, which was abolished or severely diminished in these mutants (Figs 2B,C).

Our previous results also suggested that the import of extracellular Zn^{2+} may be the source of PGRP-induced increase in intracellular free Zn^{2+}, because chelating extracellular Zn^{2+} abolished the PGRP-induced increase in intracellular free Zn^{2+} and prevented PGRP-induced killing (Kashyap *et al.*, 2011, 2014). If this was the case, we predicted that deleting Zn^{2+} importers in bacteria would diminish PGRP-induced increase in intracellular free Zn^{2+}. Indeed, PGRP-induced increase in intracellular free Zn^{2+} was significantly diminished in mutants lacking genes for Zn^{2+} importers, *znuABC* or *zupT*, and also in a double mutant lacking both Zn^{2+} importers (*znuABC* and *zupT*), in which PGRP-induced Zn^{2+} increase was reduced by 60% (Fig. 8B). By contrast, deleting other non-specific Zn^{2+} importers (*zinT, mntH*, or *pitA*) had no or little effect. These results indicate that PGRP-induced increase in intracellular free Zn^{2+} to a large extent requires import of extracellular Zn^{2+}, and that ZnuABC and ZupT importers have the greatest contribution to the PGRP-induced Zn^{2+} import. These PGRP-induced increases in Zn^{2+} were not completely abolished in *znuABC* and *zupT* mutants, because nonspecific metal importers, such as MntH and PitA, and Zn^{2+}-binding protein ZinT (Kershaw *et al.*, 2007) are able to import Zn^{2+} and may to some extent compensate in the *znuABC* and *zupT* double mutant. Because Zn^{2+} is essential for growth, mutants completely lacking all Zn^{2+} importers are not viable and cannot be obtained.

To further determine the role of Zn^{2+} import in PGRP-induced killing, we next determined the sensitivity to PGPR killing of mutants lacking the specific Zn^{2+} importers (*znuABC* and *zupT*). Mutants lacking *znuABC* or *zupT* and a double mutant lacking both *znuABC* and *zupT* were all significantly more resistant to PGRP killing (Fig. 8C), which shows that Zn^{2+} import is important for both PGRP-induced metal stress and killing.

CpxRA is a negative regulator of PGRP-induced oxidative stress, but not thiol and metal stress

We previously proposed that in *E. coli* CpxRA two-component system positively controls PGRP-induced bacterial killing, based on activation of CpxRA in PGRP-treated cells and higher resistance of *cpxA* and *cpxR* deletion mutants to PGRP killing compared with the parental MG1655 strain (Kashyap *et al.*, 2011). Therefore, here we tested whether some or all of the PGRP-induced pathways that result in oxidative, thiol, and metal stress are regulated by CpxRA.

To verify the role of CpxRA in resistance to PGRP killing, we first compared the sensitivity to PGRP killing of *cpxA* and *cpxR* deletion mutants from four sources. All four *cpxA* deletion mutants had significantly greater resistance to PGRP killing than the parental strains (Fig. 9A). By contrast, three *cpxR* deletion mutants and also our *cpxRA* mutant, all had similar sensitivity to PGRP killing as their parental strains. Only one *cpxR* deletion mutant (from Boston University) was significantly more resistant to PGRP killing than its parental strain (Fig. 9A), similar to our previously reported results for the same mutant (Kashyap *et al.*, 2011). We conclude that *cpxA*, but not *cpxR* mutants are more resistant to PGRP killing.

We next determined the role of CpxRA in PGRP-induced oxidative, thiol, and metal stress, and also in the reactions leading to the oxidative stress, using our *cpxA, cpxR*, and *cpxRA* mutants.

PGRP-induced increase in H_2O_2 production was abolished in the *cpxA* mutant, but not in the *cpxR* and *cpxRA* mutants, although it was somewhat lower in the *cpxRA* mutant than in the parental strain (Fig. 9B). PGRP treatment also did not induce an increase in NADH level and NADH/NAD^+ ratio in the *cpxA* mutant, relative to control BSA treatment, because NADH level and NADH/NAD^+ ratio were already high in BSA-treated *cpxA* mutant. By contrast, PGRP treatment induced similar increases in NADH level and NADH/NAD^+ ratio in *cpxR* and *cpxRA* mutants as in the parental strain (Fig. 9C). PGRP treatment also did not increase cAMP concentration in the *cpxA* mutant, relative to control BSA treatment, because cAMP concentration was also already high in BSA-treated *cpxA* mutant, whereas again PGRP treatment induced similar increases in cAMP concentration in *cpxR* and *cpxRA* mutants as in the parental strain (Fig. 9E). However, PEP and PEP/pyruvate ratio were only increased by PGRP treatment in the parental strain, but not in *cpxA, cpxR*, and *cpxRA* mutants (Fig. 9D). Thus, our results with H_2O_2, NADH, and cAMP production correlate well with the increased resistance to PGRP killing of *cpxA* mutant and similar sensitivity to PGRP killing of the parental strain and *cpxR* and *cpxRA* mutants. They also further confirm the requirement for oxidative stress in PGRP killing.

PGRP treatment resulted in similar 90% depletion of thiols in the parental strain and both *cpxR* and *cpxRA* mutants, and 66% depletion of thiols in *cpxA* mutant (Fig. 9F). Thus, PGRP induced significant depletion of thiols in all *cpx* mutants, although this depletion was 25% less severe in *cpxA* mutant than in the parental strain and *cpxR* and *cpxRA* mutants. These results again correlate with the increased resistance of *cpxA* mutant to PGRP killing. Deletion of *cpxA, cpxR*, or *cpxRA* had no effect on PGRP-induced increase in the intracellular free Zn^{2+} concentration (Fig. 9G).

Based on the reported constitutive activation of CpxR in the *cpxA* deletion mutant (Mahoney and Silhavy, 2013), our results suggested that activation of CpxR could significantly attenuate PGRP-induced killing and oxidative stress (H_2O_2 production and associated increase in NADH and cAMP), and partially attenuate thiol stress (depletion of thiols), but not metal stress (intracellular Zn^{2+} increase).

To verify this hypothesis, we next determined whether CpxR was indeed constitutively activated in our *cpxA* mutant, by assaying the expression of *cpxP*, a member of the CpxR regulon solely controlled by CpxR. Indeed, *cpxA* mutant had approximately 10-fold higher level of expression of *cpxP* relative to the parental strain (which was statistically significant) (Fig. 9H). Thus, these results show high constitutive activation of CpxR, regardless of the treatment with BSA (unstimulated negative control), PGRP, or gentamicin (positive control).

We have previously shown that CpxRA was activated after 60 min of PGRP treatment (Kashyap *et al.*, 2011). Here, we tested whether CpxRA was activated in PGRP-treated cells at the time of the maximum metabolic and oxidative stress response (15 min). In parental MG1655 cells, 15-min PGRP treatment increased expression of *cpxP* 2.7-fold relative to BSA treatment, which was significant, but very low, compared with over 30-fold increase in *cpxP* expression induced by gentamicin and 10-fold higher constitutive CpxR activation in the *cpxA* mutant (Fig. 9H). These results indicate only very low activation of CpxRA by PGRP at this early time point. Of note, in both *cpxR* and *cpxRA* mutants *cpxP* was not expressed, confirming the requirement for CpxR in *cpxP* expression and validating the use of *cpxP* expression as an assay for CpxR activation.

In conclusion, high constitutive activation of CpxR and no PGRP-induced production of H_2O_2 in the *cpxA* mutant indicate that CpxR is a negative regulator of PGRP-induced oxidative stress, which is the likely reason for the increased resistance of *cpxA* mutant to PGRP killing.

Discussion

Our results indicate that in *E. coli* PGRP induces increased production of H_2O_2 and oxidative stress through a block in respiratory chain, and that PGRP-induced generation of H_2O_2 depends on increased supply of NADH from cAMP-Crp-controlled glycolysis and TCA cycle (Fig. 10). Efficient respiration in growing cells with quick flow of electrons through the respiratory chain generates only very small amounts H_2O_2, because cytochromes have high affinity for O_2 and efficiently reduce O_2 to H_2O (Imlay, 2013; Karp *et al.*, 2017). Therefore, in an intact electron transport chain, a large increase in H_2O_2 production would require an equally large increase in respiration. However, PGRP induces decreased respiration with a large simultaneous increase in H_2O_2 production. How can a decreased O_2 consumption rate result in increased H_2O_2 production? To explain these results we propose that PGRP treatment causes a block in electron flow through the respiratory chain from NADH oxidoreductases to the cytochromes and O_2, leading to a backup of electrons on solvent-exposed flavin cofactors of NADH oxidoreductases. We further propose that the reduced flavins on these enzymes then auto-oxidize through adventitious contact with O_2, but because they have low affinity for O_2 and transfer only one or two electrons to

O_2, O_2 is incompletely reduced to O_2^- or H_2O_2, followed by rapid dissociation of H_2O_2 from the enzyme (Messner and Imlay, 1999; Seaver and Imlay, 2004; Esterhazy *et al.*, 2008; Imlay, 2013). Because most of the electrons backed up on the flavins are prematurely diverted to O_2, a large increase in H_2O_2 is accompanied by a decrease in total O_2 consumption. The electrons for O_2 reduction are supplied by the NADH generated from a transient increase in carbon catabolism, which could be an adaptive response of bacteria to the PGRP-induced respiratory block (Fig. 10).

Single deletions of genes for either one of the respiratory NADH oxidoreductases (*nuo* or *ndh*), or for the TCA cycle enzymes (*sucB, sucD, icd*, or *lpdA*), or *crp* or *cyaA* (positive regulators of carbon catabolism), all have similar effects of abolishing PGRP-induced H_2O_2 production (Fig. 2B,C) and decreasing bacterial killing (Fig. 1). These results suggest that NDH-2 could be the main enzyme that accepts electrons from NADH in PGRP-treated cells, consistent with high induction of *ndh* expression by PGRP treatment, and with increased NADH/NAD^+ ratio only in PGRP-treated *ndh* mutant. Thus, PGRP-treated *ndh* mutant could have a deficient generation of H_2O_2, because it lacks this main enzyme that accepts electrons from NADH used for reduction of O_2 to H_2O_2. By contrast, both TCA cycle mutants and *nuo* mutants have decreased NADH/NAD^+ ratios in PGRP-treated cells (Fig. 5A). This is consistent with the expected lower conversion of NAD^+ to NADH in TCA cycle mutants. However, we have no explanation for the decreased NADH/NAD^+ ratios in PGRP-treated *nuo* mutants. Regardless of the regulatory mechanism, this lower supply of NADH in TCA cycle and *nuo* mutants would result in a decreased transfer of electrons from NADH to NADH oxidoreductases and their lower capacity to reduce O_2 to H_2O_2. This explanation would account for deficient H_2O_2 production in *ndh, nuo*, and TCA cycle mutants and offer one possibility why *nuo* and *ndh* do not compensate for each other.

We also identified two additional flavoprotein sources of PGRP-induced H_2O_2: fumarate reductase (Frd) and choline dehydrogenase (BetA/CDH), as deletion of their genes also causes increased resistance to PGRP killing (Fig. 1A and Table S1) and diminished PGRP-induced production of H_2O_2, although significantly less than deletion of *nuo* or *ndh* (Fig. 2B). Fumarate reductase (Frd) functions mostly in anaerobic respiration, but may be a significant source of H_2O_2 under aerobic conditions (Korshunov and Imlay, 2010), as is the case here in PGRP-treated cells. BetA is another oxidoreductase linked to electron transfer and is oxygen-dependent (Landfald and Strøm, 1986). However, it is unclear how Frd and BetA function in PGRP-induced generation of H_2O_2.

In addition to oxidative stress, effective PGRP killing also requires induction of thiol and metal stress in bacteria (Kashyap *et al.*, 2014). Therefore, in this study, we also analyzed whether thiol and metal stress are induced by PGRP through the same mechanism as the oxidative stress.

Thiols maintain the redox state in the cells and protect cells from oxidative damage. Depletion of intracellular thiols, known as thiol (or disulfide) stress, can be induced by oxidative stress through ROS-mediated oxidation of thiols, or by electrophiles, such as quinones, aldehydes, and azo- or amido-compounds. These electrophiles can also induce ROS or can directly modify thiols by oxidation, alkylation, or arylation (Liebeke *et al.*,

2008; Pöther *et al.*, 2009; Müller *et al.*, 2013; Leichert *et al.*, 2003; Faulkner and Helmann, 2011).

Our results show that PGRP-induced depletion of thiols is not caused by and is mostly independent of PGRP-induced oxidative stress, because PGRP treatment of mutants with deleted respiratory chain oxidoreductases (*nuo* and *ndh*), TCA cycle enzymes (*sucB, sucD, icd*, and *lpdA*), or other oxidoreductases (*frd* and *betA*), in which PGRP-induced production of H_2O_2 was abolished or decreased, still resulted in severe depletion of intracellular thiols (Fig. 7). Oxidative-stress independence of PGRP-induced thiol stress is also supported by our previous results showing that the amount of intracellular H_2O_2 induced by PGRP in bacteria is not sufficient to significantly deplete intracellular thiols (Kashyap *et al.*, 2014). PGRP-induced depletion of thiols, however, is partially dependent on cAMP-Crp (Fig. 7), which is not surprising, because cAMP-Crp regulates over 300 genes (Görke and Stülke, 2008; Karp *et al.*, 2017; Shimada *et al.*, 2011), many of which may not be involved in oxidative stress. Because PGRP by itself is not a thiol-reactive electrophile and also because it does not enter the cytoplasm (Kashyap *et al.*, 2011), our results suggest that PGRP triggers thiol depletion through additional currently unidentified pathways. One possibility is that PGRP induces excessive production of endogenous electrophiles, such as quinones, which would then directly deplete thiols.

It is generally accepted that oxidative and thiol stress result in release of metals from proteins and/or increased metal import, which increase intracellular concentration of free metals, including Zn^{2+}, increases metal toxicity, and induce expression of genes for metal detoxification and efflux (Leichert *et al.*, 2003; Harrison *et al.*, 2009; Faulkner and Helmann, 2011). Our previous results were consistent with this notion, because PGRP induced strong oxidative, thiol, and metal stress, accompanied by a dramatic increase in intracellular free (labile) Zn^{2+} and expression of genes for the efflux and detoxification of zinc, copper, arsenite, and other metals controlled by metal-responsive or stress-responsive regulators (CueR, ArsR, SoxR, RcnR) (Kashyap *et al.*, 2014).

Thus, our original hypothesis was that PGRP-induced metal stress was a consequence of PGRP-induced oxidative and/or thiol stress. However, our subsequent and current results do not support this hypothesis and indicate that PGRP-induced increase in intracellular free Zn^{2+} is independent of PGRP-induced oxidative and thiol stress. This conclusion is based on the following results. First, neither paraquat (a direct inducer of O_2^- and H_2O_2) nor diamide (a thiol-depleting electrophile) induce any increases in intracellular Zn^{2+} in *E. coli* and *B. subtilis*, despite inducing a large increase in intracellular H_2O_2 or severe depletion of thiols (Kashyap *et al.*, 2014). And second, PGRP induces similar increases in intracellular Zn^{2+} in parental strains and in all deletion mutants lacking respiratory chain oxidoreductases (*nuo* and *ndh*), or TCA cycle enzymes (*sucB, sucD, icd*, and *lpdA*), or regulators of central carbon catabolism (*crp* and *cyaA*), or other oxidoreductases (*frd* and *betA*) (Fig. 8A), in which PGRP-induced production of H_2O_2 was abolished or decreased (Fig. 2B,C).

Our current and previous results also indicate that PGRP-induced increase in intracellular Zn^{2+} is mostly due to an influx of extracellular Zn^{2+} into the cells, rather than a release from intracellular sources, because this increase was significantly reduced in deletion mutants

lacking the ZnuABC and ZupT Zn^{2+} importers (Fig. 8B). Moreover, as already indicated, increasing intracellular H_2O_2 with paraquat or depleting intracellular thiols with diamide do not induce an increase in intracellular Zn^{2+}, which would be expected if oxidative or thiol stress were causing release of Zn^{2+} from intracellular sources. Furthermore, chelating extracellular Zn^{2+} with EGTA (whose log stability constant for Zn^{2+} is 12.9) completely prevents PGRP-induced increase in intracellular Zn^{2+} and abolishes bactericidal activity of PGRP (Wang *et al.*, 2007; Kashyap *et al.*, 2014). The requirement for influx of extracellular Zn^{2+} for PGRP killing is further demonstrated by increased resistance to PGRP killing of mutants deficient in Zn^{2+} importers (*znuABC* and *zupT*) (Fig. 8C).

CpxRA two-component system is a transmembrane sensor of envelope stress and is activated by a variety of insults, including misfolded proteins in the periplasm and in the cytoplasmic and outer membranes, alterations in membrane proteins, lipids, or peptidoglycan, and also by many other stresses, such as pH, metals, osmolarity, adhesion, EDTA, indole, ethanol, other metabolites, and PGRPs (Zhou *et al.*, 2011; Hunke *et al.*, 2012; Raivio, 2014; Evans *et al.*, 2013; Bernal-Cabas *et al.*, 2015; Keller *et al.*, 2015; Delhaye *et al.*, 2016; Kashyap *et al.*, 2011). However, the exact mechanism of CpxRA activation by such a large variety of stimuli still remains elusive (Raivio, 2014; Delhaye *et al.*, 2016).

Here we show that CpxR, constitutively activated in the *cpxA* mutant, is a negative regulator of PGRP-induced increases in H_2O_2, NADH, NADH/NAD^+ ratio, and cAMP. By contrast, PGRP-induced thiol stress is mostly insensitive, and PGRP-induced increase in intracellular Zn^{2+} is completely insensitive to this negative regulation by CpxR. Although we previously reported that PGRP activates CpxRA, this activation occurs late, at 60 min of PGRP exposure (Kashyap *et al.*, 2011), which is much too late to prevent PGRP-induced H_2O_2 production that peaks at 15 min of PGRP exposure (Fig. 2A). For this reason CpxRA does not protect parental cells from PGRP-induced oxidative stress and killing (unless CpxR is artificially pre-activated by *cpxA* deletion).

Our results suggest that PGRP induces oxidative, thiol, and metal stress through three independent pathways. These results are consistent with our previous and current data showing that inhibiting one stress (oxidative, thiol, or metal) with chemical inhibitors makes PGRPs only bacteriostatic or less bactericidal (Kashyap *et al.*, 2011, 2014), and that single deletion mutants can only be partially, but not fully, resistant to PGRP killing. The reason for this partial resistance is that these inhibitors or single mutations can only disable one stress pathway, which only reduces, but does not completely abolish antibacterial activity of PGRP, as each stress on its own is bacteriostatic, and combining two and three stresses progressively amplifies their antibacterial effect (Kashyap *et al.*, 2014). This strategy assures that these innate immune proteins, conserved in evolution from insects to mammals, do not easily lose their antibacterial activity.

The proposed subsequent steps that lead to PGRP-induced bacterial death after induction of oxidative, thiol, and metal stress, include: (i) generation of toxic $HO^{\bullet}$ from H_2O_2, which starts at 30 min and peaks in 2–3 hrs of PGRP exposure (likely involving Fe^{2+} from Fe-S clusters as an electron donor) and damages bacterial DNA (Kashyap *et al.*, 2011); (ii) cessation of all biosynthetic reactions in bacteria, which starts at 30 min of PGRP exposure

(Kashyap *et al.*, 2011), likely due to the lack of energy following a decrease in respiration rate and catabolism, which happen within 30 min of PGRP exposure (Fig. 6); and (iii) membrane depolarization, which starts at 1 hr and peaks at 2–3 hrs of PGRP exposure (Kashyap *et al.*, 2011), likely due to decrease in proton translocation by respiratory chain and energy depletion. These events are irreversible, because diluting bacteria into a fresh medium at 2–3 hrs does not allow for their growth, although these bacteria are still not dead even at 6 hrs of PGRP exposure, because their membranes are still not permeabilized (Wang *et al.*, 2007; Kashyap *et al.*, 2011).

Manipulations of bacterial metabolism and ROS production are often studied with a goal to enhance effectiveness of antibiotics. Increased carbon catabolism and respiration are associated with bacterial killing by bactericidal antibiotics (Dwyer *et al.*, 2014; Belenky *et al.*, 2015; Lobritz *et al.*, 2015). Similar to our results with PGRP, *E. coli* deletion mutants in TCA cycle genes are more resistant to antibiotic killing than parental strains (Kohanski *et al.*, 2007). However, opposite effects of metabolism on the sensitivity to antibiotics were also reported, as deleting respiratory chain or TCA cycle genes enhanced sensitivity to exogenous oxidants and β-lactam and fluoroquinolone antibiotics (Brynildsen *et al.*, 2013). By contrast, in our experiments similar mutations enhanced resistance to PGRP, because respiratory chain and TCA cycle are required to generate PGRP-induced oxidative stress. Increased bacterial killing by aminoglycoside antibiotics in bacteria with enhanced TCA cycle and respiration was due a greater uptake of aminoglycosides driven by increased proton motive force (Allison *et al.*, 2011; Peng *et al.*, 2015). Furthermore, treatment of *E. coli* with bactericidal antibiotics induced a transient 5-fold decrease in the $NADH/NAD^+$ ratio (Kohanski *et al.*, 2007), whereas PGRP induced a transient increase in $NADH/NAD^+$ ratio (Fig. 4A). Also, bactericidal antibiotics increased O_2 consumption rate (Lobritz *et al.*, 2015), whereas PGRP, which is also bactericidal, decreased it (Fig. 6). Moreover, many effects of antibiotics on the metabolism seem to be the consequences or indirect responses to the primary effects of antibiotics, as they happen late in antibiotic-induced killing (30 to 90 min) (Kohanski *et al.*, 2007; Belenky *et al.*, 2015). By contrast, the kinetics of PGRP-induced changes in metabolism and respiration reported here are much faster (5 min). These changes are the first detectable effects of PGRP, which argues for the block in respiratory chain and increased catabolism as the primary effects of PGRP on bacteria. There are many additional differences between bacterial killing by PGRP and antibiotics, which were discussed previously (Kashyap *et al.*, 2011, 2014).

In conclusion, in *E. coli* bactericidal PGRP induces severe oxidative stress through a block in respiratory chain, which likely diverts electrons from respiratory chain NADH oxidoreductases to O_2, generates H_2O_2, and results in decreased respiration. Production of H_2O_2 depends on increased supply of NADH from cAMP-Crp-controlled glycolysis and TCA cycle (Fig. 10). CpxRA two-component system is a negative regulator of PGRP-induced oxidative stress. PGRP also induces thiol stress and metal stress, which are mostly independent of oxidative stress and CpxRA. Manipulating these pathways that induce oxidative, thiol, and metal stress in bacteria could be a useful strategy to design new approaches to antibacterial therapy.

Experimental Procedures

Materials

Human recombinant PGLYRP4 was used as a representative bactericidal PGRP, as we have previously shown that all human bactericidal PGRPs had similar activity and the mechanism of bacterial killing (Lu *et al.*, 2006; Wang *et al.*, 2007; Kashyap *et al.*, 2011, 2014). PGLYRP4 was expressed in S2 cells and purified as previously described (Lu *et al.*, 2006; Wang *et al.*, 2007) in a buffer containing 10 mM TRIS (pH 7.6), with 150 mM NaCl, 10 μM $ZnSO_4$, and 10% glycerol. Paraquat (methyl viologen) was from Acros Organics. Fatty acids-free purified bovine serum albumin (BSA, used as a negative control), and other reagents were from Sigma-Aldrich, unless otherwise indicated.

Bacteria, growth, and media

The entire Keio collection of 3884 *E. coli* K-12 in-frame single-gene knockout mutants was obtained from the National BioResource Project, National Institute of Genetics, Japan (Baba *et al.*, 2006). Individual *E. coli* strains used in this study are listed in Table S3 (Baba *et al.*, 2006; Yun *et al.*, 2005; Kohanski *et al.*, 2008; Sabri *et al.*, 2009; Mahoney and Silhavy, 2013). Bacteria were grown aerobically overnight at 37°C in an orbital shaker (250 rpm) in LB, diluted to OD_{660} = 0.02 into fresh LB and grown to OD_{660} = 0.6. Bacteria were centrifuged and suspended in the “Assay Medium”, which was the same for all the killing or metabolic experiments here and in our previous killing experiments on *E. coli* (Wang *et al.*, 2007; Kashyap *et al.*, 2011, 2014). This Assay Medium contained (final concentrations): 5 mM TRIS (pH 7.6) with 2.5% glycerol, 150 mM NaCl, 5 μM $ZnSO_4$, and 2% of 100% LB. *E. coli* MG1655 generation time in this assay medium at 37°C was 30 min. The change in the medium from LB to the Assay Medium did not create any significant stress for bacteria, as they immediately (within <1 min) resume their metabolic activity, as measured by respiration and extracellular acidification rates (Fig. 6A,B), and placing the cells in this medium did not induce oxidative, thiol, or metal stress. Also, pre-incubation of cells in this medium for 30 min did not change their response to PGRP, as measured by respiration, extracellular acidification rate, H_2O_2 production, and killing.

Screening of Keio collection for mutants resistant to PGRP killing

To screen the entire *E. coli* Keio library of 3884 single gene deletion mutants to find mutants with increased resistance to PGRP killing, we grew each mutant aerobically at 37°C on a shaker in 100 μl of LB in 96-well plates to an average approximate OD_{660} of 0.12. Then we pooled equal volumes of cultures of 10–12 mutants, and treated 20 μl of each pool of mutants diluted 1:2000 times into the Assay Medium in a 96-well plate with 100 μg/ml human PGRP aerobically for 3 hrs at 37°C, which is sufficient to kill over 99.5% of *E. coli* K-12 strain. We then added 180 μl of fresh LB into each well with the treated pools of mutants, re-incubated them at 37°C aerobically, and measured the growth of surviving bacteria by following changes in optical density (OD_{660}) every 10 min for 16 hrs. This method yielded growth curves for each pool of mutants and the curves with accelerated growth reflected either more bacteria that survived PGRP killing or presence of faster growing mutants in this pool (Fig. S1A). We then selected 24 pools of mutants with the most accelerated growth curves for the second round of screening, which was performed the same

as the first screening described above, but in this screening to prepare the cultures of pooled mutants, the same numbers of bacteria for each mutant added to each pool were used, calculated based on OD_{660} of each mutant culture. This assured starting PGRP treatment with the same numbers of each mutant in each pool and minimized the effect of differences in the rate of growth of mutants. Then at the end of 3 hrs of PGRP treatment, the numbers of bacteria in each pool were determined by colony counts and compared with the numbers of surviving bacteria in similarly prepared and treated isogenic BW25113 parental strain (Fig. S1B). From this second screening we then selected three pools of mutants with the highest numbers of surviving bacteria with mutant pool/parental strain ratios of 20, 15, and 13 (pools 14, 7, and 13 in Fig. S1B). We then compared PGRP killing of all mutants from these three pools to the killing of the BW25113 parental strain, using colony counts for each mutant grown individually after 3 hrs of treatment with 200 μg/ml PGRP. We also screened by colony counts individual mutants from six additional mutant pools that had the ratios of surviving mutants to parental strain between 8 and 10 (pools 9, 17, 18, 20, 22, and 24 in Fig. S1B), concentrating on mutants for respiratory chain enzymes, TCA cycle enzymes, and several other oxidoreductases, because most of the more resistant mutants belonged to these categories. Out of all the mutants individually tested by colony counts for increased resistance to PGRP killing, there were 14 mutants with statistically significant higher survival than the parental strain and the ratio of survival of PGRP-treated Δ mutant *versus* parental strain of >10. These mutants are shown in Fig. 1A and Table S1.

PGRP killing assay

E. coli were grown as described above in “Bacteria, growth, and media” section and suspended at ~10^6 bacteria/ml in 50 μl of fresh warm Assay Medium (5 mM TRIS, pH 7.6, with 150 mM NaCl, 5 μM $ZnSO_4$, 2.5% glycerol, with 2% of 100% LB) with addition of 100 μg/ml BSA or PGRP and incubated at 37°C aerobically with 250 rpm shaking for 3 hrs. The numbers of bacteria were then determined by colony counts (Kashyap *et al.*, 2011, 2014). Bactericidal activity is defined as an at least 100-fold decrease in the number of inoculated bacteria in 3 hrs.

Construction and verification of deletion mutants

We created gene deletion mutants (Table S3) by replacing the entire coding sequence of the genes with kanamycin resistance cassette using homologous recombination. First, we generated PCR fragments using primers (Table S4) and methodology described by Baba *et al.* (2006). Briefly, the N-terminal deletion primers had a 50-nt 5’ extension including the gene initiation codon (H1) and a 20-nt sequence 5’-ATTCCGGGGATCCGTCGACC-3’ (P1). The C-terminal deletion primers consisted of 21 nt for the C-terminal region, the termination codon, and 29-nt downstream (H2), and the 20-nt sequence 5’-TGTAGGCTGGAGCTGCTTCG-3’ (P2). PCR reactions were run for 30 cycles in 50 μl volumes using Advantage 2 polymerase (Clontech), 1 ng DNA from individual mutants from the Keio collection, 0.4 μM of each primer, and 200 mM dNTPs. PCR products were digested with *Dpn*I, gel purified, and suspended in nuclease free water. Gene disruption was carried out by the method of Datsenko and Wanner (2000), with slight modifications. Briefly, *E. coli* MG1655 carrying the Red helper plasmid pKD46 (CGSC # 7669) was grown in 5-ml SOB culture with ampicillin and L-arabinose at 30°C overnight. Next day, the

culture was diluted to OD_{660} = 0.02 in fresh SOB medium and allowed to grow to OD_{600} = 0.6. Electro-competent cells were made by concentrating the cells 100-fold and washing three times with ice-cold 10% glycerol. Electroporation was done in Gen Pulser Xcell™ electroporation system (Bio-Rad) according to the manufacturer's instructions by using 50 μl of cells and 10–100 ng of *Dpn*I-treated gel-purified PCR product. Transformed cells were recovered in SOC media with ampicillin and L-arabinose at 30°C while shaking, overnight. The next morning, the transformation mix was spread on LB agar plates with 30 μg/ml kanamycin. Resistant colonies were picked after overnight incubation at 37°C. Removal of the pKD46 plasmid was confirmed by the lack of growth on LB/Amp plates at 30°C. The correct chromosomal deletions were first verified by colony PCR. A freshly isolated colony was suspended in 10 μl nuclease free water and 5 μl of this bacterial suspension was used for two 25 μl PCRs following a 4-min hot-start at 94°C with kanamycin-specific primers kan-F or kan-R and gene-specific primers F or R (Table S4) as described by Datsenko and Wanner (2000). The gene deletions in each mutant were then further verified by capillary sequencing using gene-specific F and R primers.

H_2O_2 assay

H_2O_2 production was measured by a modification of our previous assay using Amplex Red Hydrogen Peroxide/Peroxidase Assay Kit (InVitrogen/Molecular Probes), based on enzymatic detection of H_2O_2 by horseradish peroxidase (Kashyap *et al.*, 2014). *E. coli* were grown and suspended in 50 μl of Assay Medium at OD_{660} = 0.15 as described above in "Bacteria, growth, and media" section, with addition of 100 μg/ml BSA (control) or PGRP, or 100 μM paraquat. Bacteria were then incubated aerobically at 37°C on a shaker for 15 min (unless otherwise indicated). The reactions were then stopped by lysing bacteria with 40 mM HEPES, 4 mM EDTA, 400 mM KCl, 0.2% Triton X-100, pH 8.1 in a bath sonicator on ice for 5 min, and total amount of H_2O_2 was determined by measuring fluorescence according to the manufacturer's instructions. In this procedure, detection of H_2O_2 after quick lysis of bacteria does not require the use of Hpx^- mutant *E. coli* strain, which we used previously (Kashyap *et al.*, 2014). H_2O_2 concentration was calculated from a standard curve and reported as μM (μmol/liter) for the original bacterial incubation mixture.

NADH and NAD^+ assays

E. coli were grown and suspended in 150 μl of Assay Medium at OD_{660} = 0.3 as described above in "Bacteria, growth, and media" section, with addition of 100 μg/ml BSA (control) or PGRP. Bacteria were incubated aerobically at 37°C on a shaker for 15 min (unless otherwise indicated), 100 μl was used for NADH and 50 μl for NAD^+ assay. The reactions were stopped by addition of 100 mM NaOH for NADH assay or 100 mM HCl for NAD^+ assay in 40 mM HEPES, 4 mM EDTA, 400 mM KCl, 0.2% Triton X-100, and the cells were sonicated and heated at 60°C for 5 min. Then, NADH or NAD^+ concentrations were determined using EnzyChrom NAD^+/NADH Assay Kit (BioAssay Systems) according to the manufacturer's instructions. The assay is based on lactate dehydrogenase cycling reaction, in which NADH reduces a formazan reagent. NADH and NAD^+ concentrations were calculated from a standard curve and reported as μM (μmol/liter) for the original bacterial incubation mixture.

Phosphoenolpyruvate (PEP) and pyruvate assays

E. coli were grown and suspended in 100 μl of Assay Medium at OD_{660} = 0.15 as described above in "Bacteria, growth, and media" section, with addition of 100 μg/ml BSA (control) or PGRP. Bacteria were incubated aerobically at 37°C on a shaker for 5 min (unless otherwise indicated). The reactions were then stopped by adding ice-cold 3 M $HClO_4$ and vortexing, followed by neutralization with 3 M $KHCO_3$. The concentrations of extracted PEP and pyruvate were then measured in the cell lysates using PEP Fluorometric Assay Kit and Pyruvate Fluorometric Assay Kit (BioVision), respectively, according to the manufacturer's instructions. PEP and pyruvate concentrations were calculated from a standard curve and reported as μM (μmol/liter) for the original bacterial incubation mixture.

cAMP assay

E. coli were grown and suspended in 50 μl of Assay Medium at OD_{660} = 0.15 as described above in "Bacteria, growth, and media" section, with addition of 100 μg/ml BSA (control) or PGRP. Bacteria were incubated aerobically at 37°C on a shaker for 5 min (unless otherwise indicated). The reactions were then stopped by adding lysis buffer (40 mM HEPES, 4 mM EDTA, 400 mM KCl, 0.2% Triton X-100) and boiling for 5 min. Then, cAMP concentrations were determined using luminescent cAMP-Glo™ Assay Kit (Promega) according to the manufacturer's instructions. The assay is based on specific activation of protein kinase A by cAMP. cAMP concentration was calculated from a standard curve and reported as nM (nmol/liter) for the original bacterial incubation mixture.

Thiols assay

Depletion of thiols (all reduced sulfhydryl groups) was measured as previously described (Kashyap *et al.*, 2014). *E. coli* were grown and suspended in 50 μl of Assay Medium at OD_{660} = 0.15 as described above in "Bacteria, growth, and media" section, with addition of 100 μg/ml BSA (control) or PGRP. Bacteria were incubated aerobically at 37°C on a shaker for 30 min. The reactions were then stopped by lysing bacteria with 40 mM HEPES, 4 mM EDTA, 400 mM KCl, 0.2% Triton X-100, pH 8.1 in a bath sonicator on ice for 5 min, and total amounts of reduced thiols were determined using fluorescent Measure-iT Thiol Assay Kit (InVitrogen/Molecular Probes) according to the manufacturer's instructions. Total concentration of thiols was calculated from a standard curve using glutathione and reported as μM (μmol/liter) for the original bacterial incubation mixture.

Zn^{2+} assay

Intracellular free (labile) Zn^{2+} was measured as previously described (Kashyap *et al.*, 2014). *E. coli* were grown and suspended in 50 μl of Assay Medium to ~2×10^7 *E. coli*/ml as described above in "Bacteria, growth, and media" section, with addition of 100 μg/ml BSA (control) or PGRP. Bacteria were incubated aerobically at 37°C on a shaker for 2 hrs. Bacteria were then washed and incubated with Zinpyr-1 (from Santa Cruz, dissolved in DMSO with 20% Pluronic F-127, 5 μM final concentration) for 15 min at 37°C. Bacteria were then washed and analyzed by flow cytometry using MACSQuant (Miltenyi) flow cytometer and FITC excitation and emission settings. The results are reported as mean fluorescence intensity (MFI) ± SEM, normalized for the bacterial cell size, measured by

forward scatter (FSC-A), as described below. We performed several controls to verify that our results truly reflect changes in intracellular free Zn^{2+} concentration. (i) We previously confirmed the linearity of Zn^{2+} detection with Zinpyr-1 by spiking our bacteria-PGRP mixtures with different ratios of free Zn^{2+} and EDTA (a divalent chelator with high affinity for Zn^{2+} with 16.6 log dissociation constant), and assaying Zn^{2+} concentrations using the Zinpyr-1 probe and fluorescence spectroscopy (with Molecular Devices Gemini EM Spectrofluorimeter). The detected Zn^{2+} concentrations were in good agreement with the calculated free Zn^{2+} concentrations (Kashyap *et al.*, 2014). (ii) We excluded the possibility that increased intracellular Zinpyr-1 accumulation was due to an increase in membrane permeability following PGRP treatment, because we previously reported that treatment with bactericidal concentration of PGRP did not increase membrane permeability for at least 6 hrs in *E. coli* (Wang *et al.*, 2007) or in Gram-positive bacteria (Lu *et al.*, 2006; Kashyap *et al.*, 2011). (iii) We previously confirmed that the fluorescent signal is due to increase in intracellular Zn^{2+} that enters the cells from outside, using membrane-permeable and membrane non-permeable Zn^{2+} chelators and adding extracellular Zn^{2+} (Kashyap *et al.*, 2014). (iv) Bacterial cell filamentation or other increase in cell volume, often caused by many antibiotics, can result in increased fluorophore signal per cell when measured by flow cytometry (Paulander *et al.*, 2014). For this reason, here we verified by dark field microscopy that treatment of *E. coli* with 100 μg/ml of PGRP for 2 hrs at 37°C had no effect on the bacterial shape and size, compared with BSA-treated *E. coli* (Fig. S5). Increased cell volume could be also due to osmotic swelling that precedes osmotic lysis, but PGRPs do not induce osmotic lysis of bacteria either (Lu *et al.*, 2006; Wang *et al.*, 2007; Kashyap *et al.*, 2011). Nevertheless, to correct for any possible changes in the cell volume in PGRP-treated bacteria, here we normalized the Zinpyr-1 fluorescence signals to the cell size, as measured by FSC-A, by multiplying fluorescence signal for PGRP-treated cells by the ratio of median FSC-A for BSA-treated cells to median FSC-A for PGRP-treated cells.

Gene expression arrays

Preparation of the whole genome expression arrays was described previously (Kashyap *et al.*, 2014) and the entire data for all the arrays were deposited in NCBI GEO with accession number GSE44211 (http://www.ncbi.nlm.nih.gov/geo/query/acc.cgi?acc=GSE44211). Here, from these arrays, we present and analyze the expression in PGRP-treated *E. coli* of up-regulated and down-regulated genes for the central carbon catabolism, which are the subject of this study and were not analyzed previously. Briefly, exponentially growing *E. coli* MG1655 were suspended in the Assay Medium at OD_{660} = 0.3 as in “Bacteria, growth, and media” section, and incubated aerobically at 37°C with 100 μg/ml albumin (control) or PGRP (PGLYRP4) with 250 rpm shaking. RNA was then extracted using Ambion RiboPure-bacteria RNA extraction kit, cDNA was synthesized with random hexamer primers, fragmented, labeled with terminal transferase and biotin, and hybridized to whole genome Affymetrix *E. coli* Genome 2.0 Array GPL3154 using Affymetrix Hybridization Oven 640 and Affymetrix GeneChip Fluidics Station 450 and protocols provided by Affymetrix GeneChip Technical Manual. Scanning and data extraction were done using Affymetrix GeneChip Scanner 3000 and protocols provided by Affymetrix GeneChip Technical Manual. cDNA synthesis, labeling, hybridization, and scanning were performed at the Genomic and RNA Profiling Core facility, Baylor College of Medicine, Houston, TX. The entire

experiment was repeated 3 times. Hybridization intensity data signals were normalized and analyzed as described (Kashyap *et al.*, 2014) using Affymetrix GeneChip Command Console Software. Signal intensities from 3 experiments were used to calculate fold increases or decreases in gene expression between treated and control groups, and the fold changes in gene expression were calculated using the formula: intensity in treated group/ geometric mean of intensity in control (albumin) groups, and reported as means ± SEM. Transformed Ln(signal intensity) values were used for direct statistical comparisons of expression signals between treated and control (albumin) groups.

qRT-PCR

The amounts of mRNA for individual genes were measured using quantitative reverse transcription real-time PCR (qRT-PCR) as previously described (Kashyap *et al.*, 2014). *E. coli* (300 μl), grown and prepared as in "Bacteria, growth, and media" section, were incubated in the Assay Medium with 100 μg/ml BSA (control), 100 μg/ml PGRP, or 5 μg/ml gentamicin aerobically at 37°C on a shaker for 15 min, and RNA was extracted as described above for gene expression arrays. cDNA was synthesized from 100 ng of RNA using RT^2 PCR Array First Strand Kit (Qiagen). Gene expression was quantified by qRT-PCR using the ABI 7900 Sequence Detection System with 1 cycle 10-min at 95°C and 40 cycles 15 sec at 95°C and 1 min at 60°C using Qiagen SYBR Green Master Mix and the gene-specific primers (listed in Table S4) or common primers for 16S rRNA from all Eubacteria (ACTCCTACGGGAGGCAGCAGT and ATTACCGCGGCTGCTGGC) as a housekeeping gene. For each gene, ΔCt was calculated followed by normalization to the housekeeping gene, followed by calculation of ΔΔCt for each gene: ΔΔCt = ΔCt1 − ΔCt2, where ΔCt1 is the PGRP-treated bacteria and ΔCt2 is BSA-treated bacteria. This calculation gives the fold increase in expression of each gene in PGRP-treated bacteria *versus* BSA-treated bacteria. For expression of *cpxP*, ΔCt1 was the measured sample, and ΔCt2 was the background without RNA, which reflects absolute amount of *cpxP* RNA in arbitrary units. Each entire experiment was repeated 4 times.

Annotation of gene functions and regulation

The functions of genes and gene regulons were annotated using the following web databases: EcoCyc: http://biocyc.org/ECOLI/organism-summary, and RegulonDB: http://regulondb.ccg.unam.mx/index.jsp.

Oxygen consumption and extracellular acidification

O_2 consumption rate (OCR, which reflects total aerobic respiration) and extracellular acidification rate (ECAR, which reflects total H^+ production from carbon catabolism) were measured simultaneously in real time with the Seahorse XFp analyzer (Agilent Technologies), which uses label-free, solid-state sensor cartridges in a microplate format (Lobritz *et al.*, 2015; Saini *et al.*, 2016). First, to attach bacteria to the XFp cell culture microplates, the plates were coated for 20 minutes at room temperature with 25 μl/well of BD Cell-Tak Cell and Tissue Adhesive™ (BD Biosciences, prepared by diluting 46 μl of Cell-Tak into 3 ml of 0.1 M $NaHCO_3$ and then neutralizing it with ½ volume 1 N HCl), followed by rinsing the wells twice with 200 μl of sterile distilled H_2O and then drying the wells at room temperature for 20 min. *E. coli* MG1655 were grown and diluted to OD_{660nm}

= 0.0125 with warm Assay Medium (5 mM TRIS pH 7.6 with 2.5% glycerol, 150 mM NaCl, 5 μM $ZnSO_4$, and 2% of 100% LB) as described in "Bacteria, growth, and media" section, and 40 μl/well of bacteria was dispensed into the Cell-Tak-coated wells (2×10^6 bacteria per well). The bacteria were then sedimented by centrifugation at 2270 g for 2 min, BSA (control) or PGRP were added to a final concentration of 100 μg/ml, and incubation at 37°C and OCR and ECAR measurements were started immediately. The micro-chamber wells are automatically re-equilibrated and oxygenated between measurements through the up and down mixing by the probes of the XFp sensor cartridge. The results are reported as mean ± SEM OCR (in pmol/min) and ECAR (in mpH/min) for the original bacterial incubation mixture, and also as phenograms of OCR plotted versus ECAR that illustrate the total cell energy phenotype.

Statistical analyses

Quantitative results are presented as means ± SEM, with statistical significance of the differences between groups determined by the two-sample one-tailed Student's *t*-test or one-sample Student's *t*-test using Microsoft Excel; $P \leq 0.05$ was considered significant. The *n* and *P* values are indicated in the figures and tables. Gene expression results are presented as heat maps generated using Java TreeView and represent mean fold changes in gene expression in PGRP-treated relative to BSA-treated bacteria, after converting <1 ratios to negative fold difference using the formula: (−1)/ratio. For microarray data statistical significance of differences in gene expression was also analyzed by calculating *P* values using two-sample two-tailed Student's *t*-test, followed by calculation of $\pi_0(\lambda)$ and then FDR (false discovery rate) *q* values, with significance threshold of $q \leq 0.05$, as described (Storey and Tibshirani, 2003).

Supplementary Material

Refer to Web version on PubMed Central for supplementary material.

Acknowledgments

We are grateful to George N. Bennett, Charles M. Dozois, Sebastien Houle, James J. Collins, Michael A. Kohanski, Thomas J. Silhavy, and Tara F. Mahoney for *E. coli* strains, to James A. Imlay and Christopher Rensing for helpful comments, to Sarah S. Iqbal for help with experiments, and to Iztok Hozo for help with statistical analysis. This study was supported by grants AI028797, AI073290, and AI120962 from United States Public Health Service National Institutes of Health (to R.D.).

References

Allison KR, Brynildsen MP, Collins JJ. Metabolite-enabled eradication of bacterial persisters by aminoglycosides. Nature. 2011; 473:216–220. [PubMed: 21562562]

Baba T, Ara T, Hasegawa M, Takai Y, Okumura Y, Baba M, et al. Construction of *Escherichia coli* K-12 in-frame, single-gene knockout mutants: the Keio collection. Mol Syst Biol. 2006; 2 2006.0008.

Belenky P, Ye JD, Porter CB, Cohen NR, Lobritz MA, Ferrante T, et al. Bactericidal antibiotics induce toxic metabolic perturbations that lead to cellular damage. Cell Rep. 2015; 13:968–980. [PubMed: 26565910]

Bernal-Cabas M, Ayala JA, Raivio T. The Cpx envelope stress response modifies peptidoglycan cross-linking via the L,D-transpeptidase LdtD and the novel protein YgaU. J Bacteriol. 2015; 197:603–614. [PubMed: 25422305]

Brynildsen MP, Winkler JA, Spina CS, MacDonald IC, Collins JJ. Potentiating antibacterial activity by predictably enhancing endogenous microbial ROS production. Nat Biotechnol. 2013; 31:160–165. [PubMed: 23292609]

Cochemé HM, Murphy MP. Complex I is the major site of mitochondrial superoxide production by paraquat. J Biol Chem. 2008; 283:1786–1798. [PubMed: 18039652]

Datsenko KA, Wanner BL. One-step inactivation of chromosomal genes in *Escherichia coli* K-12 using PCR products. Proc Natl Acad Sci USA. 2000; 97:6640–6645. [PubMed: 10829079]

Delhaye A, Collet JF, Laloux G. Fine-tuning of the Cpx envelope stress response is required for cell wall homeostasis in *Escherichia coli*. MBio. 2016; 7 pii: e00047–16.

Dwyer DJ, Belenky PA, Yang JH, MacDonald IC, Martell JD, Takahashi N, et al. Antibiotics induce redox-related physiological alterations as part of their lethality. Proc Natl Acad Sci USA. 2014; 111:E2100–2109. [PubMed: 24803433]

Dwyer DJ, Collins JJ, Walker GC. Unraveling the physiological complexities of antibiotic lethality. Annu Rev Pharmacol Toxicol. 2015; 55:313–332. [PubMed: 25251995]

Dziarski, R., Royet, J., Gupta, D. Peptidoglycan recognition proteins and lysozyme. In: Ratcliffe, MJH., editor. Encyclopedia of Immunobiology. Vol. 2. Elsevier; 2016. p. 389-403.

Eppler T, Postma P, Schütz A, Völker U, Boos W. Glycerol-3-phosphate-induced catabolite repression in *Escherichia coli*. J Bacteriol. 2002; 184:3044–3052. [PubMed: 12003946]

Esterhazy D, King MS, Yakovlev G, Hirst J. Production of reactive oxygen species by complex I (NADH:ubiquinone oxidoreductase) from *Escherichia coli* and comparison to the enzyme from mitochondria. Biochemistry. 2008; 47:3964–3971. [PubMed: 18307315]

Evans KL, Kannan S, Li G, de Pedro MA, Young KD. Eliminating a set of four penicillin binding proteins triggers the Rcs phosphorelay and Cpx stress responses in *Escherichia coli*. J Bacteriol. 2013; 195:4415–4424. [PubMed: 23893115]

Ezraty B, Vergnes A, Banzhaf M, Duverger Y, Huguenot A, Brochado AR, et al. Fe-S cluster biosynthesis controls uptake of aminoglycosides in a ROS-less death pathway. Science. 2013; 340:1583–1587. [PubMed: 23812717]

Faulkner MJ, Helmann JD. Peroxide stress elicits adaptive changes in bacterial metal ion homeostasis. Antioxid Redox Signal. 2011; 15:175–189. [PubMed: 20977351]

Gelius E, Persson C, Karlsson J, Steiner H. A mammalian peptidoglycan recognition protein with *N*-acetylmuramoyl-L-alanine amidase activity. Biochem Biophys Res Commun. 2003; 306:988–994. [PubMed: 12821140]

Görke B, Stülke J. Carbon catabolite repression in bacteria: many ways to make the most out of nutrients. Nat Rev Microbiol. 2008; 6:613–624. [PubMed: 18628769]

Harrison JJ, Tremaroli V, Stan MA, Chan CS, Vacchi-Suzzi C, Heyne BJ, et al. Chromosomal antioxidant genes have metal ion-specific roles as determinants of bacterial metal tolerance. Environ Microbiol. 2009; 11:2491–2509. [PubMed: 19555372]

Hunke S, Keller R, Müller VS. Signal integration by the Cpx-envelope stress system. FEMS Microbiol Lett. 2012; 326:12–22. [PubMed: 22092888]

Imlay JA. The molecular mechanisms and physiological consequences of oxidative stress: lessons from a model bacterium. Nat Rev Microbiol. 2013; 11:443–454. [PubMed: 23712352]

Imlay JA. Diagnosing oxidative stress in bacteria: not as easy as you might think. Curr Opin Microbiol. 2015; 24:124–131. [PubMed: 25666086]

Karp, PD., Keseler, I., Fulcher, C., Kothari, A., Paley, S., Krummenacker, M., et al. Summary of *Escherichia coli*, strain K-12 substr. MG1655, version 21.0. 2017. EcoCyc: http://biocyc.org/ECOLI/

Kershaw CJ, Brown NL, Hobman JL. Zinc dependence of zinT (yodA) mutants and binding of zinc, cadmium and mercury by ZinT. Biochem Biophys Res Commun. 2007; 364:66–71. [PubMed: 17931600]

Kashyap DR, Wang M, Liu L-H, Boons G-J, Gupta D, Dziarski R. Peptidoglycan recognition proteins kill bacteria by activating protein-sensing two-component systems. Nature Med. 2011; 17:676–683. [PubMed: 21602801]

Kashyap DR, Rompca A, Gaballa A, Helmann JD, Chan J, Chang CJ, et al. Peptidoglycan recognition proteins kill bacteria by inducing oxidative, thiol, and metal stress. PLoS Pathog. 2014; 10:e1004280. [PubMed: 25032698]

Keller R, Ariöz C, Hansmeier N, Stenberg-Bruzell F, Burstedt M, Vikström D, et al. The *Escherichia coli* envelope stress sensor CpxA responds to changes in lipid bilayer properties. Biochemistry. 2015; 54:3670–3676. [PubMed: 25993101]

Keren I, Wu Y, Inocencio J, Mulcahy LR, Lewis K. Killing by bactericidal antibiotics does not depend on reactive oxygen species. Science. 2013; 339:1213–1216. [PubMed: 23471410]

Kohanski MA, Dwyer DJ, Hayete B, Lawrence CA, Collins JJ. A common mechanism of cellular death induced by bactericidal antibiotics. Cell. 2007; 130:797–810. [PubMed: 17803904]

Kohanski MA, Dwyer DJ, Wierzbowski J, Cottarel G, Collins JJ. Mistranslation of membrane proteins and two-component system activation trigger antibiotic-mediated cell death. Cell. 2008; 135:679–690. [PubMed: 19013277]

Korshunov S, Imlay JA. Two sources of endogenous hydrogen peroxide in *Escherichia coli*. Mol Microbiol. 2010; 75:1389–1401. [PubMed: 20149100]

Landfald B, Strøm AR. Choline-glycine betaine pathway confers a high level of osmotic tolerance in *Escherichia coli*. J Bacteriol. 1986; 165:849–855. [PubMed: 3512525]

Leichert LIO, Scharf C, Hecker M. Global characterization of disulfide stress in *Bacillus subtilis*. J Bacteriol. 2003; 185:1967–1975. [PubMed: 12618461]

Liebeke M, Pöther DC, van Duy N, Albrecht D, Becher D, Hochgräfe F, et al. Depletion of thiol-containing proteins in response to quinones in *Bacillus subtilis*. Mol Microbiol. 2008; 69:1513–1529. [PubMed: 18673455]

Liu Y, Imlay JA. Cell death from antibiotics without the involvement of reactive oxygen species. Science. 2013; 339:1210–1213. [PubMed: 23471409]

Lobritz MA, Belenky P, Porter CB, Gutierrez A, Yang JH, Schwarz EG, et al. Antibiotic efficacy is linked to bacterial cellular respiration. Proc Natl Acad Sci USA. 2015; 112:8173–8180. [PubMed: 26100898]

Lu X, Wang M, Qi J, Wang H, Li X, Gupta D, Dziarski R. Peptidoglycan recognition proteins are a new class of human bactericidal proteins. J Biol Chem. 2006; 281:5895–5907. [PubMed: 16354652]

Mahoney TF, Silhavy TJ. The Cpx stress response confers resistance to some, but not all, bactericidal antibiotics. J Bacteriol. 2013; 195:1869–1874. [PubMed: 23335416]

Messner KR, Imlay JA. The identification of primary sites of superoxide and hydrogen peroxide formation in the aerobic respiratory chain and sulfite reductase complex of *Escherichia coli*. J Biol Chem. 1999; 274:10119–10128. [PubMed: 10187794]

Müller A, Hoffmann JH, Meyer HE, Narberhaus F, Jakob U, Leichert LIO. Non native disulfide bond formation activates the σ^{32}-dependent heat shock response in *Escherichia coli*. J Bacteriol. 2013; 195:2807–2816. [PubMed: 23585533]

Paulander W, Wang Y, Folkesson A, Charbon G, Løbner-Olesen A, Ingmer H. Bactericidal antibiotics increase hydroxyphenyl fluorescein signal by altering cell morphology. PLoS One. 2014; 9:e92231. [PubMed: 24647480]

Peng B, Su YB, Li H, Han Y, Guo C, Tian YM, Peng XX. Exogenous alanine and/or glucose plus kanamycin kills antibiotic-resistant bacteria. Cell Metab. 2015; 21:249–261. [PubMed: 25651179]

Pöther DC, Liebeke M, Hochgräfe F, Antelmann H, Becher D, Lalk M, et al. Diamide triggers mainly S thiolations in the cytoplasmic proteomes of *Bacillus subtilis* and *Staphylococcus aureus*. J Bacteriol. 2009; 191:7520–7530. [PubMed: 19837798]

Raivio TL. Everything old is new again: an update on current research on the Cpx envelope stress response. Biochim Biophys Acta. 2014; 1843:1529–1541. [PubMed: 24184210]

Royet J, Dziarski R. Peptidoglycan recognition proteins: pleiotropic sensors and effectors of antimicrobial defenses. Nature Rev Microbiol. 2007; 5:264–277. [PubMed: 17363965]

Sabri M, Houle S, Dozois CM. Roles of the extraintestinal pathogenic Escherichia coli ZnuACB and ZupT zinc transporters during urinary tract infection. Infect Immun. 2009; 77:1155–1164. [PubMed: 19103764]

Saini V, Cumming BM, Guidry L, Lamprecht DA, Adamson JH, Reddy VP, et al. Ergothioneine maintains redox and bioenergetic homeostasis essential for drug susceptibility and virulence of *Mycobacterium tuberculosis*. Cell Rep. 2016; 14:572–585. [PubMed: 26774486]

Seaver LC, Imlay JA. Are respiratory enzymes the primary sources of intracellular hydrogen peroxide? J Biol Chem. 2004; 279:48742–48750. [PubMed: 15361522]

Sharma P, Dube D, Singh A, Mishra B, Singh N, Sinha M, et al. Structural basis of recognition of pathogen-associated molecular patterns and inhibition of proinflammatory cytokines by camel peptidoglycan recognition protein. J Biol Chem. 2011; 286:16208–16217. [PubMed: 21454594]

Shimada T, Fujita N, Yamamoto K, Ishihama A. Novel roles of cAMP receptor protein (CRP) in regulation of transport and metabolism of carbon sources. PLoS One. 2011; 6:e20081. [PubMed: 21673794]

Storey JD, Tibshirani R. Statistical significance for genomewide studies. Proc Natl Acad Sci USA. 2003; 100:9440–9445. [PubMed: 12883005]

Tran QH, Bongaerts J, Vlad D, Unden G. Requirement for the proton-pumping NADH dehydrogenase I of *Escherichia coli* in respiration of NADH to fumarate and its bioenergetic implications. Eur J Biochem. 1997; 244:155–160. [PubMed: 9063459]

Tydell CC, Yount N, Tran D, Yuan J, Selsted ME. Isolation, characterization, and antimicrobial properties of bovine oligosaccharide-binding protein. A microbicidal granule protein of eosinophils and neutrophils. J Biol Chem. 2002; 277:19658–19664. [PubMed: 11880375]

Tydell CC, Yuan J, Tran P, Selsted ME. Bovine peptidoglycan recognition protein-S: antimicrobial activity, localization, secretion and binding properties. J Immunol. 2006; 176:1154–1162. [PubMed: 16394004]

Wang Z-M, Li X, Cocklin RR, Wang M, Wang M, Fukase K, et al. Human peptidoglycan recognition protein-L is an *N*-acetylmuramoyl-L-alanine amidase. J Biol Chem. 2003; 278:49044–49052. [PubMed: 14506276]

Wang M, Liu LH, Wang S, Li X, Lu X, Gupta D, Dziarski R. Human peptidoglycan recognition proteins require zinc to kill both Gram-positive and Gram-negative bacteria and are synergistic with antibacterial peptides. J Immunol. 2007; 178:3116–3125. [PubMed: 17312159]

Yun NR, San KY, Bennett GN. Enhancement of lactate and succinate formation in adhE or pta-ackA mutants of NADH dehydrogenase-deficient *Escherichia coli*. J Appl Microbiol. 2005; 99:1404–1412. [PubMed: 16313413]

Zhou X, Keller R, Volkmer R, Krauss N, Scheerer P, Hunke S. Structural basis for two-component system inhibition and pilus sensing by the auxiliary CpxP protein. J Biol Chem. 2011; 286:9805–9814. [PubMed: 21239493]

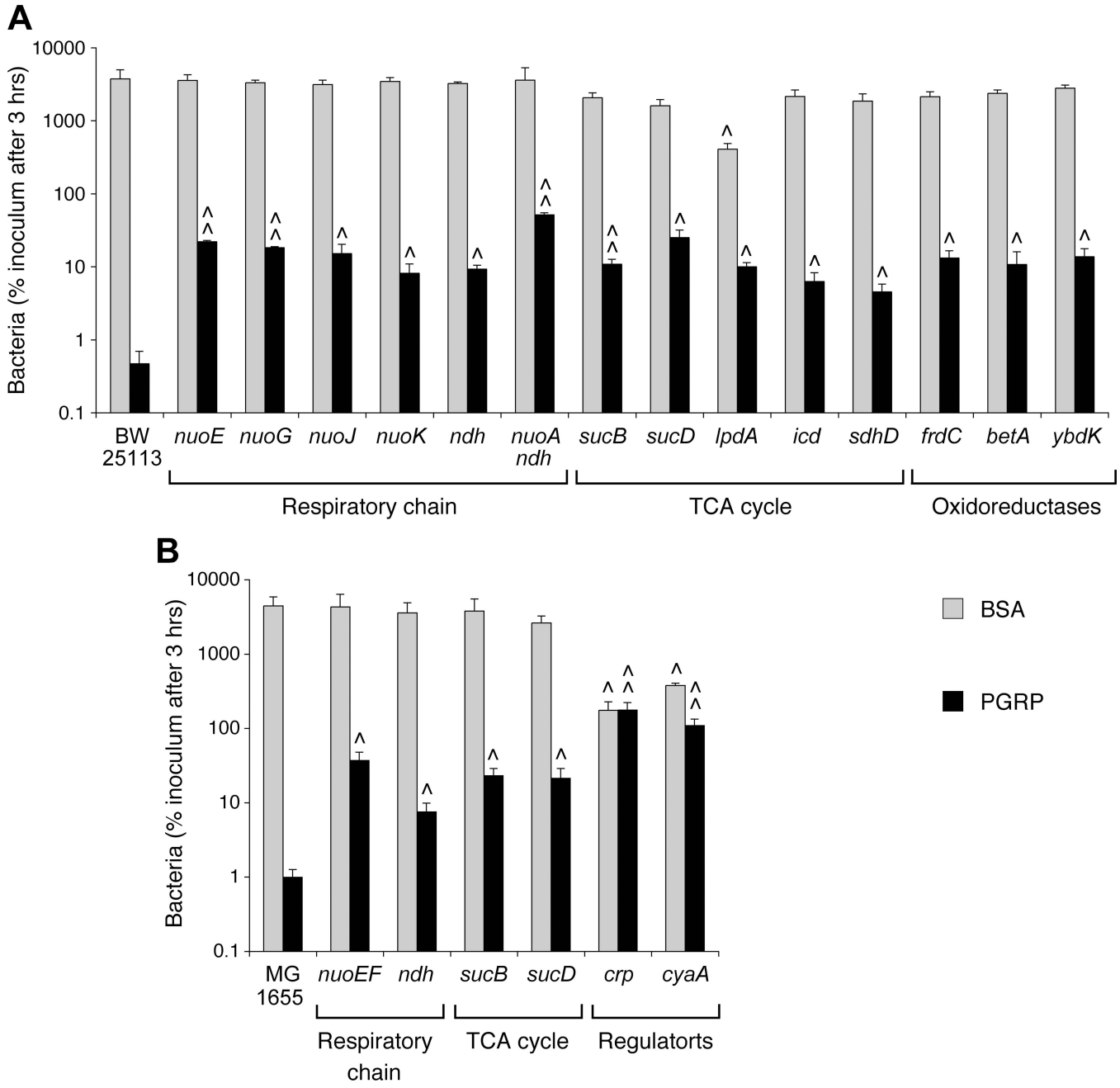

Fig. 1. *E. coli* mutants with increased resistance to PGRP killing revealed by screening of Keio library

(**A**) Mutants with increased resistance to PGRP killing were identified by three-stage screening of the entire Keio collection of single gene deletion mutants (Fig. S1 and Table S1) and here the survival of the parental strain (BW25113) and mutants following 3-hr incubation with 200 μg/ml of BSA (as a control) or PGRP is shown. Gene products, their functions, and numerical data are shown in Table S1. (**B**) Mutants for the key genes for the respiratory chain and TCA cycle, and their regulators (*cyaA* and *crp*) were constructed in MG1655 and their sensitivity to killing by 100 μg/ml of PGRP was similarly tested. The results are means of 3 experiments, expressed as percent of initial inoculum (100%) + SEM;

^ $P \leq 0.05$, ^^ $P < 0.001$, numbers of viable bacteria (colony forming units) of Δ mutants *versus* parental strain (*t*-test).

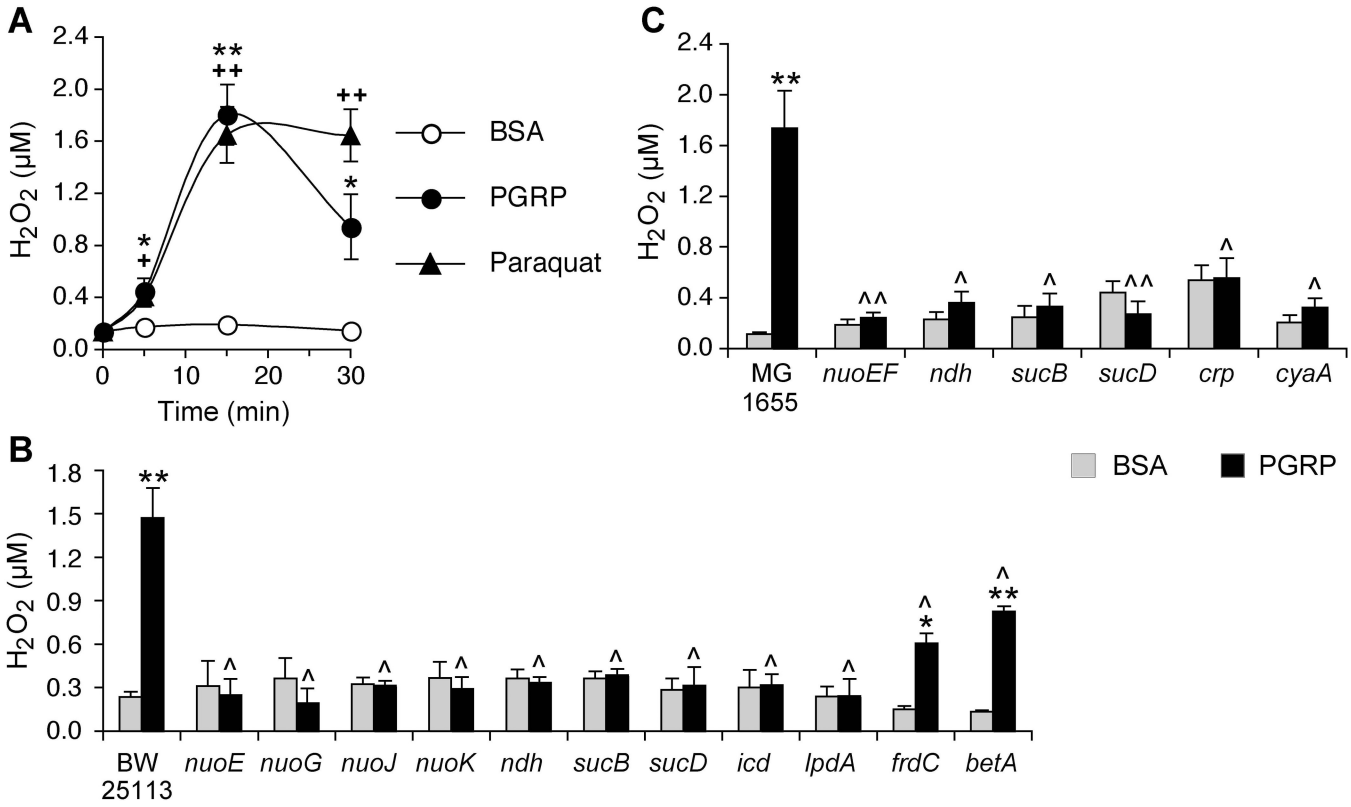

Fig. 2. H_2O_2 production in PGRP-treated *E. coli*

(**A**) Time kinetics of changes of H_2O_2 in *E. coli* MG1655 treated with 100 μg/ml BSA or PGRP, or with 100 μM paraquat. (**B**) H_2O_2 in *E. coli* BW25113 and in the indicated deletion mutants from Keio collection treated with 100 μg/ml BSA or PGRP for 15 min. (**C**) H_2O_2 in *E. coli* MG1655 and in the indicated deletion mutants constructed in our laboratory treated with 100 μg/ml BSA or PGRP for 15 min. The results are means of 3–4 experiments ± SEM (SEM were within symbols if not visible); * $P<0.05$, ** $P<0.001$, PGRP *vs* BSA; $^{+}P<0.05$, $^{++}P<0.001$, paraquat *vs* BSA; ^ $P<0.05$, ^^ $P<0.001$, PGRP-treated mutant *vs* parental strain.

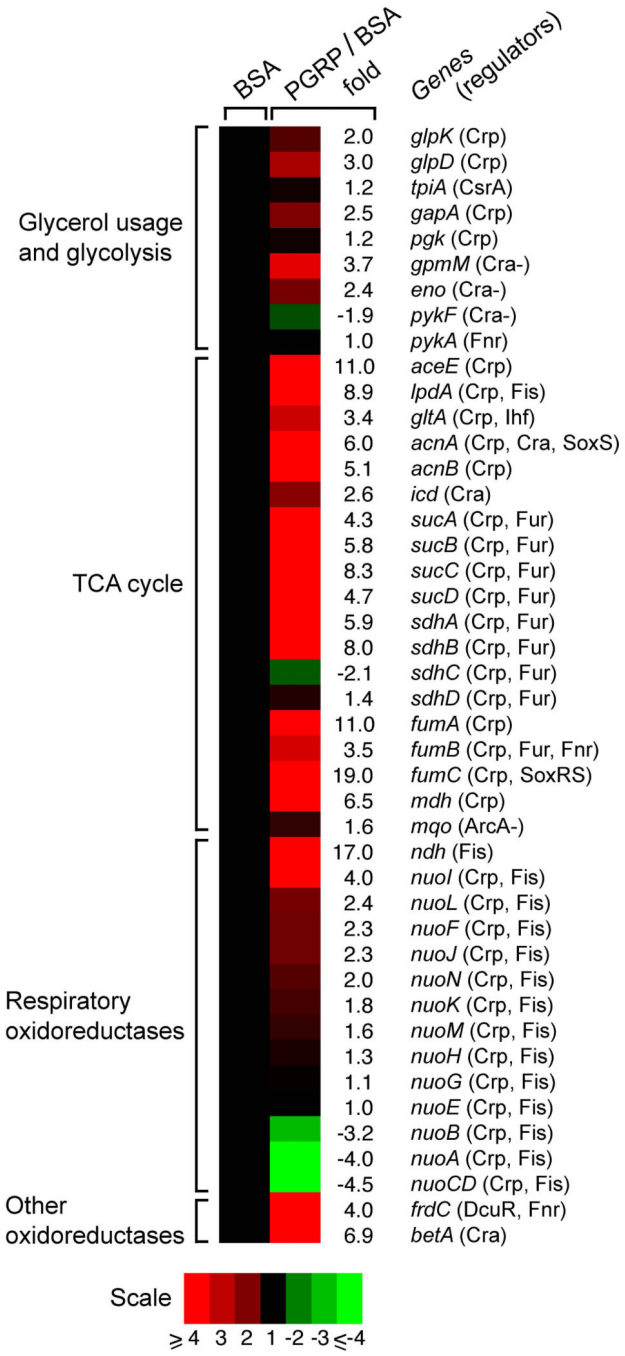

Fig. 3. PGRP treatment of *E. coli* up-regulates genes for central carbon catabolism and respiratory chain

E. coli MG1655 was treated with 100 μg/ml BSA or PGRP for 30 min and the fold increase in gene expression was determined by whole genome expression arrays. The results are means of 3 experiments and the quantitative expression data, the significance of differences, the gene functions are shown in Table S2, and the reactions catalyzed by gene products for glycerol usage in glycolysis and TCA cycle are shown in Fig. S2. The entire genome expression array data were deposited in NCBI GEO (accession number GSE44211).

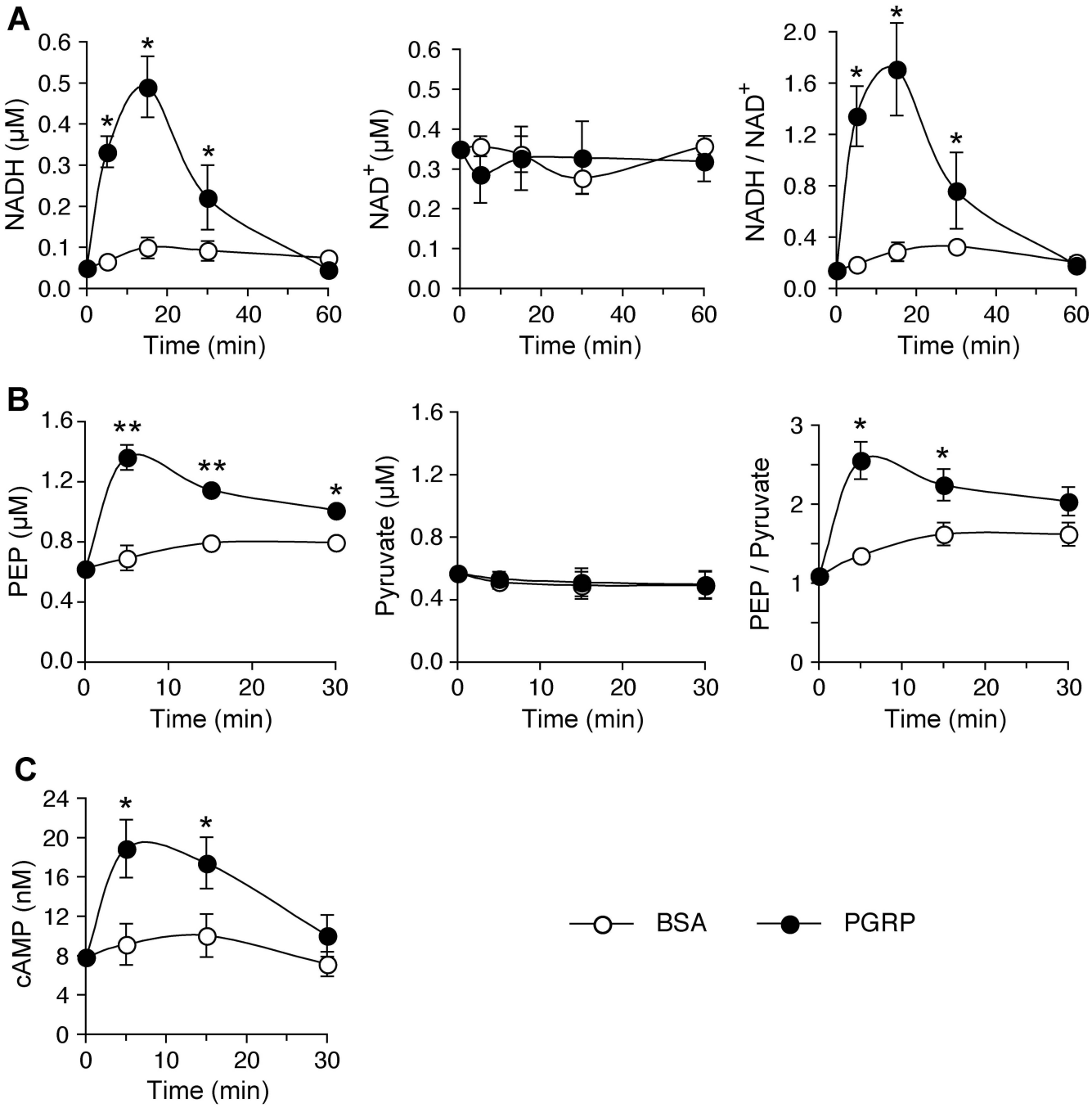

Fig. 4. Time kinetics of changes in NADH, NAD^+ and NADH/NAD^+ ratio (A), phosphoenolpyruvate (PEP), pyruvate, and PEP/pyruvate ratio (B), and cAMP (C) in PGRP-treated *E. coli*

E. coli MG1655 was treated with 100 μg/ml BSA or PGRP. The results are means of 3–4 experiments ± SEM (SEM were within symbols if not visible); * $P<0.05$, ** $P<0.001$, PGRP *vs* BSA.

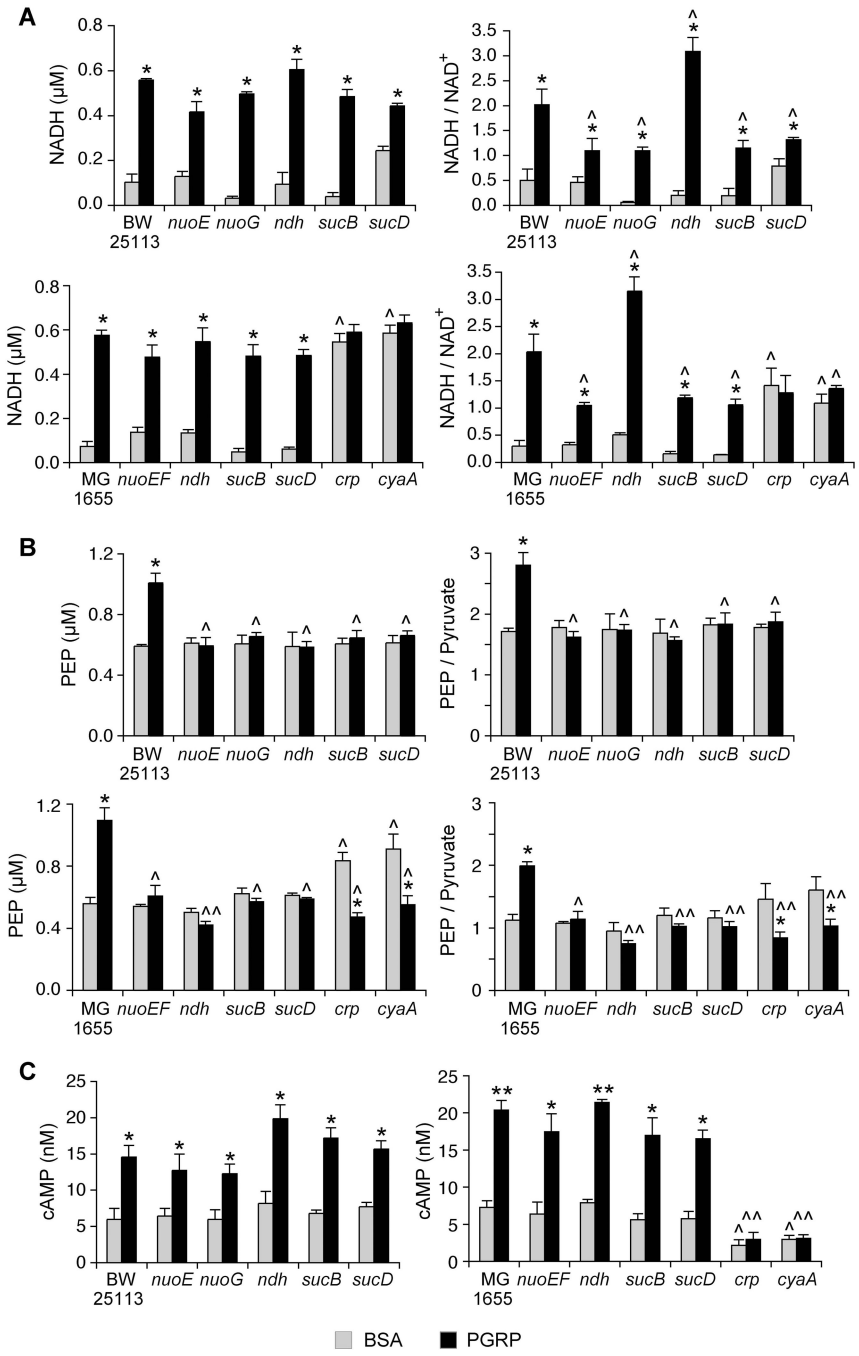

Fig. 5. NADH, NAD$^+$ and NADH/NAD$^+$ ratio (A), phosphoenolpyruvate (PEP), pyruvate, and PEP/pyruvate ratio (B), and cAMP (C) in PGRP-treated *E. coli* mutants

Parental *E. coli* or the indicated deletion mutants from Keio collection (BW25113) or from our laboratory (MG1655) were treated with 100 μg/ml BSA or PGRP for 15 min (A) or 5 min (B and C). The results are means of 3–4 experiments + SEM; * P<0.05, ** P<0.001, PGRP *vs* BSA; ^ P<0.05, ^^ P<0.001, mutant *vs* parental strain.

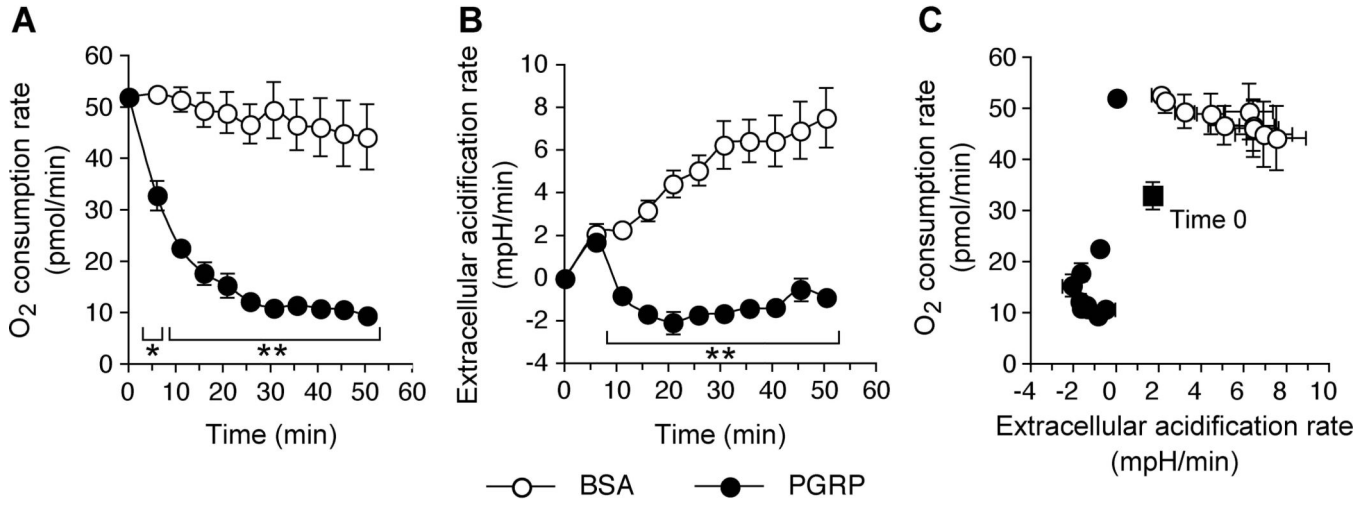

Fig. 6. Oxygen consumption and extracellular acidification rates in PGRP-treated *E. coli*

(**A**) O_2 consumption rate and (**B**) extracellular acidification rate were measured simultaneously in real time with the Seahorse XFp analyzer in *E. coli* MG1655 treated with 100 μg/ml BSA or PGRP. (**C**) A phenogram of O_2 consumption rate plotted *versus* extracellular acidification rate illustrates the total cell energy phenotype. The results are means of 6 experiments ± SEM (SEM were within symbols if not visible); * $P<0.05$, ** $P<0.0001$, PGRP *vs* BSA.

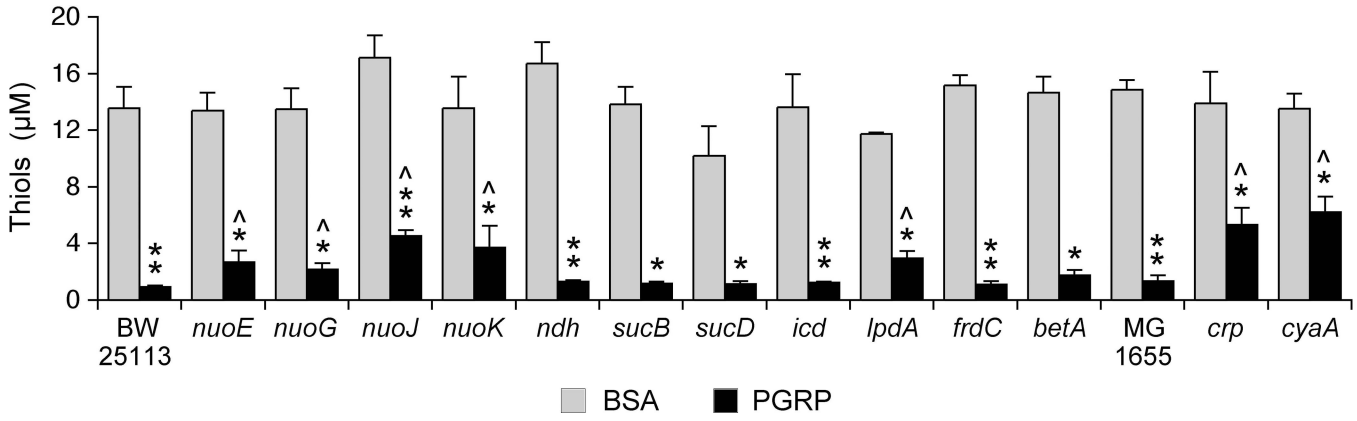

Fig. 7. Depletion of thiols in PGRP-treated *E. coli*

E. coli and the indicated deletion mutants from Keio collection (BW25113) or from our laboratory (MG1655) were treated with 100 μg/ml BSA or PGRP for 30 min. The results are means of 3 experiments + SEM; * $P<0.05$, ** $P<0.001$, PGRP *vs* BSA; ^ $P<0.05$, mutant *vs* parental strain.

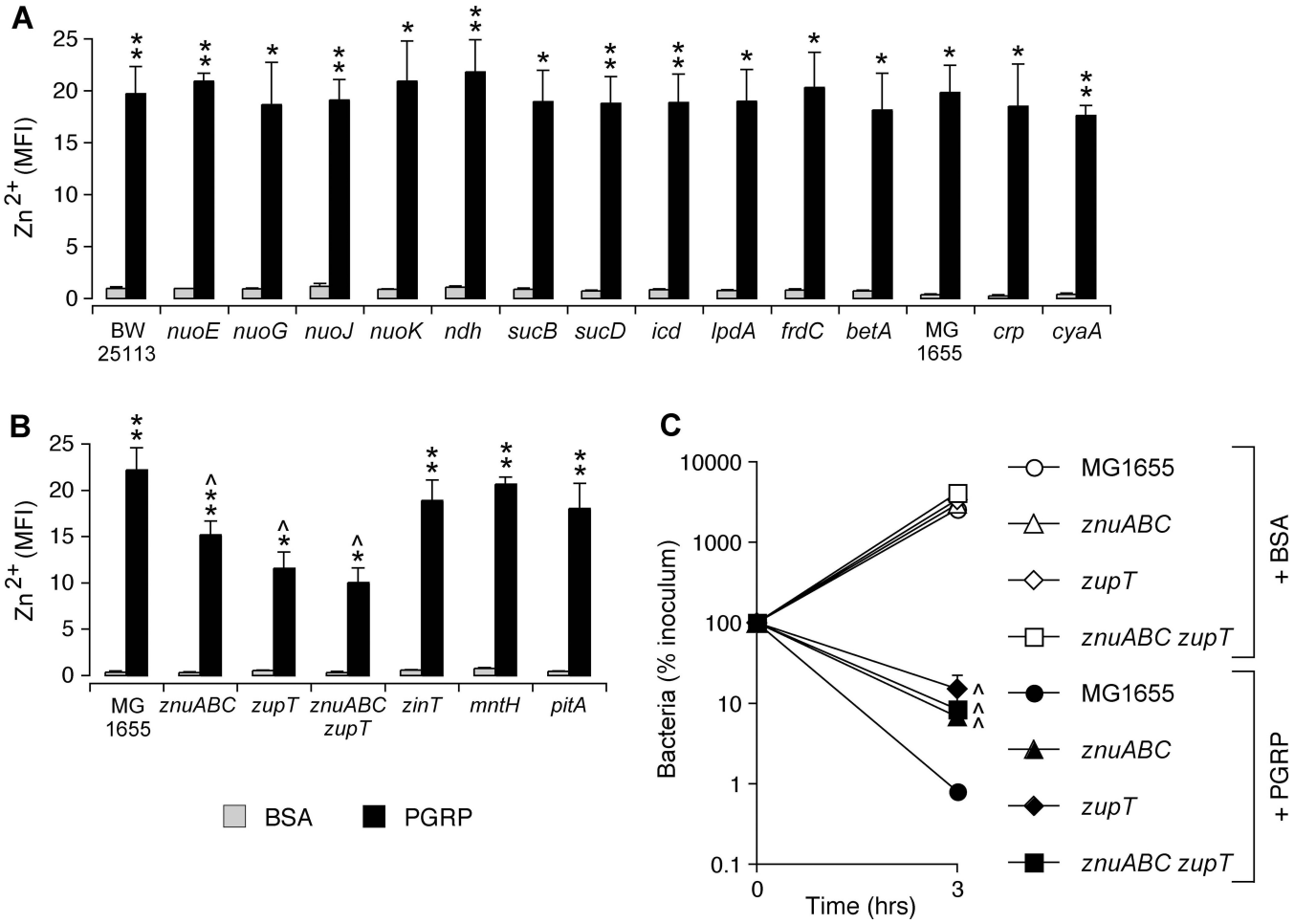

Fig. 8. Increase in intracellular free Zn^{2+} in PGRP-treated *E. coli* and increased resistance of Zn^{2+} importer mutants to PGRP killing

(**A, B**) *E. coli* BW25113 and MG1655 and the indicated deletion mutants were treated with 100 μg/ml BSA or PGRP for 2 hrs and intracellular free Zn^{2+} concentration was measured by flow cytometry with Zinpyr-1 probe. The results are shown as mean fluorescence intensity (MFI) of 3 experiments + SEM. (**C**) *E. coli* MG1655 or the indicated deletion mutants for Zn^{2+} importer genes were treated with 100 μg/ml of BSA or PGRP and the numbers of surviving bacteria were determined by colony counts. The results are expressed as percent of initial inoculum (100%) and are means of 3 experiments ± SEM (SEM were within symbols if not visible). * $P<0.05$, ** $P<0.001$, PGRP *vs* BSA; ^ $P<0.05$, PGRP-treated mutant *vs* parental strain.

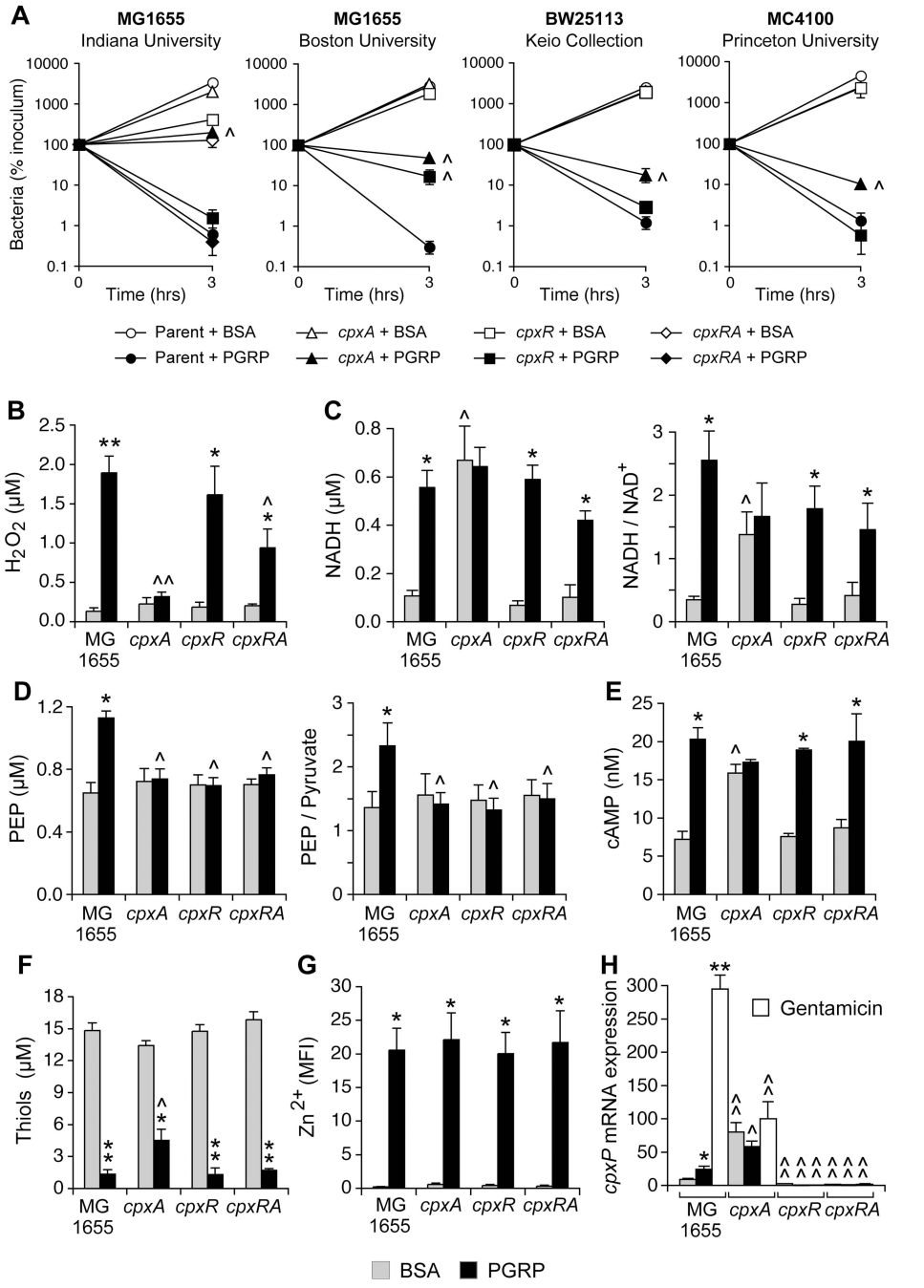

Fig. 9. CpxRA is a negative regulator of PGRP-induced killing and oxidative stress, but not thiol and metal stress

(**A**) Parental *E. coli* or *cpxA, cpxR*, and *cpxRA* deletion mutants from the indicated sources were treated with BSA or PGRP (at 100 μg/ml for MG1655 and BW25113, or 300 μg/ml for MC4100) and the numbers of surviving bacteria were determined by colony counts. The parental strains had different sensitivity to PGRP killing (Fig. S4), which was the reason for using different concentrations of PGRP to obtain similar killing of the parental strains. The results are expressed as percent of initial inoculum (100%) and are means of 4 experiments ± SEM (SEM were within symbols if not visible). (**B–H**) *E. coli* MG1655 and *cpxA, cpxR*,

and *cpxRA* deletion mutants from our laboratory were treated with 100 μg/ml BSA or PGRP and assayed for H_2O_2 (at 15 min, **B**), or NADH and NADH/NAD^+ ratios (at 15 min, **C**), or phosphoenolpyruvate (PEP) and PEP/pyruvate ratios (at 5 min, **D**), or cAMP (at 5 min, **E**), or thiols (at 30 min, **F**), or intracellular free Zn^{2+} (at 2 hrs, **G**), or *cpxP* expression (at 15 min, **H**). The results are means of 3–4 experiments + SEM. ^ $P<0.05$, ^^ $P<0.001$, mutant *vs* parental strain; * $P<0.05$, ** $P<0.001$, PGRP *vs* BSA.

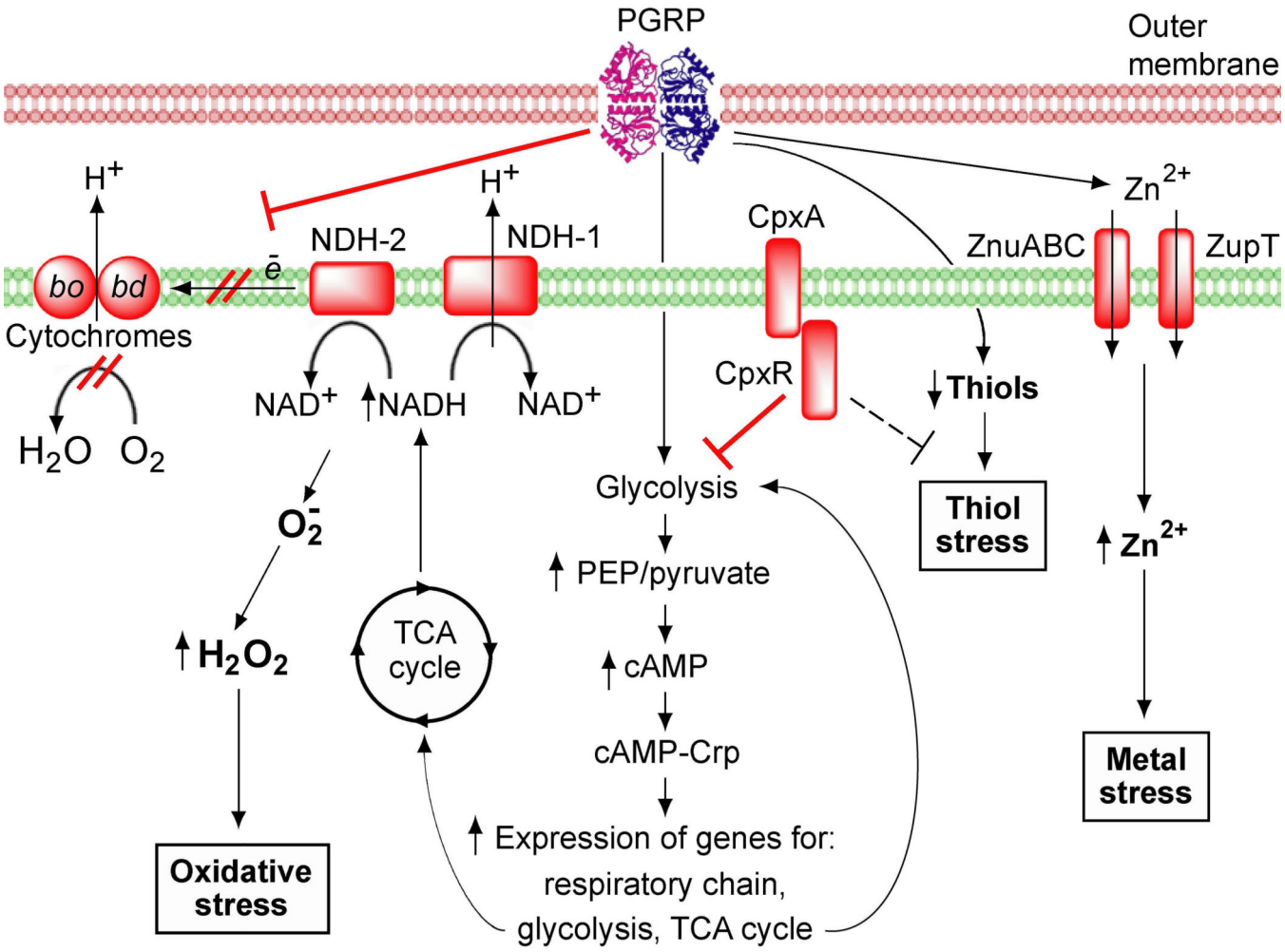

Fig. 10. Proposed pathways leading to PGRP-induced oxidative, thiol, and metal stress in *E. coli*

Bactericidal PGRP induces oxidative stress through a block in respiratory chain, which likely diverts electrons from respiratory chain NADH oxidoreductases to O_2, generates H_2O_2, and results in decreased respiration. Production of H_2O_2 depends on increased supply of NADH from cAMP-Crp-controlled glycolysis and TCA cycle. CpxRA two-component system is a negative regulator of PGRP-induced oxidative stress. PGRP-induced thiol stress (depletion of thiols) and metal stress (increase in intracellular free Zn^{2+} through influx of extracellular Zn^{2+}) are mostly independent of oxidative stress. This proposed sequence of events was determined by epistatic and biochemical analyses and does not necessarily reflect direct interactions. Broken line indicates a partial effect.